The Astrophysical Journal, 698:2048–2065, 2009 June 20 doi:10.1088/0004-637X/698/2/2048

A LARGE SAMPLE STUDY OF RED GIANTS IN THE GLOBULAR CLUSTER OMEGA CENTAURI (NGC 5139)

Christian I. Johnson[1], Catherine A. Pilachowski[1], R. Michael Rich[2], and Jon P. Fulbright[3,4]
[1] Department of Astronomy, Indiana University, Swain West 319, 727 East Third Street, Bloomington, IN 47405-7105, USA; cijohnson@astro.indiana.edu, catyp@astro.indiana.edu
[2] Department of Physics and Astronomy, UCLA, 430 Portola Plaza, Box 951547, Los Angeles, CA 90095-1547, USA; rmr@astro.ucla.edu
[3] Department of Physics and Astronomy, Johns Hopkins University, Baltimore, MD 21218, USA; jfulb@skysrv.pha.jhu.edu
Received 2009 February 17; accepted 2009 April 24; published 2009 June 5

ABSTRACT

We present abundances of several light, α, Fe-peak, and neutron-capture elements for 66 red giant branch (RGB) stars in the Galactic globular cluster Omega Centauri (ω Cen). Our observations lie in the range $12.0 < V < 13.5$ and focus on the intermediate and metal-rich RGBs. Abundances were determined using equivalent width measurements and spectrum synthesis analyses of moderate resolution ($R \approx 18{,}000$) spectra obtained with the Blanco 4 m telescope and Hydra multifiber spectrograph. Combining these data with previous work, we find that there are at least four peaks in the metallicity distribution function at [Fe/H] = −1.75, −1.45, −1.05, and −0.75, which correspond to about 55%, 30%, 10%, and 5% of our sample, respectively. Additionally, the most metal-rich stars are the most centrally located. Na and Al are correlated despite exhibiting star-to-star dispersions of more than a factor of 10, but the distribution of those elements appears to be metallicity dependent and are divided at [Fe/H] ≈ −1.2. About 40%–50% of stars with [Fe/H] < −1.2 have Na and Al abundances consistent with production solely in Type II supernovae and match observations of disk and halo stars at comparable metallicity. The remaining metal-poor stars are enhanced in Na and Al compared to their disk and halo counterparts and are mostly consistent with predicted yields from >5 $M_{\odot}$ asymptotic giant branch (AGB) stars. At [Fe/H] > −1.2, more than 75% of the stars are Na/Al enhanced and may have formed almost exclusively from AGB ejecta. Most of these stars are enhanced in Na by at least 0.2 dex for a given Al abundance than would be expected based on "normal" globular cluster values. All stars in our sample are α-rich with $\langle$[Ca/Fe]$\rangle$ = +0.36 (σ = 0.09) and $\langle$[Ti/Fe]$\rangle$ = +0.23 (σ = 0.14). The Fe-peak elements give solar-scaled abundances and similarly small dispersions with $\langle$[Sc/Fe]$\rangle$ = +0.09 (σ = 0.15) and $\langle$[Ni/Fe]$\rangle$ = −0.04 (σ = 0.09). Europium does not vary extensively as a function of metallicity and has $\langle$[Eu/Fe]$\rangle$ = +0.19 (σ = 0.23). However, [La/Fe] varies from about −0.4 to +2 and stars with [Fe/H] $\gtrsim$ −1.5 have [La/Eu] values indicating domination by the *s*-process. A quarter of our sample have [La/Eu] $\geqslant$ +1 and may be the result of mass transfer in a binary system. We conclude that the metal-rich population must be at least 1–2 Gyr younger than the metal-poor stars, owing to the long timescales needed for strong *s*-process enrichment and the development of a large contingent of mass transfer binaries.

Key words: globular clusters: general – globular clusters: individual (omega Centauri, NGC 5139) – stars: abundances – stars: Population II

Online-only material: color figures, machine-readable tables

1. INTRODUCTION

Among all of the known Galactic globular clusters, Omega Centauri (ω Cen) is unique in the extent of its chemical enrichment. The cluster exhibits huge star-to-star abundance variations that are not limited solely to the light elements, as is the case for most "normal" globular clusters. Instead, ω Cen stars have [X/Fe][5] dispersions of 0.5 to more than 1.0 dex for many elements and span a metallicity range from [Fe/H] ≈ −2.2 to nearly −0.5 (e.g., Norris & Da Costa 1995; Suntzeff & Kraft 1996; Smith et al. 2000; Johnson et al. 2008). Additionally, ω Cen's red giant branch (RGB) and subgiant branch (SGB) show 4–5 discrete populations in concert with multiple main sequences (Lee et al. 1999; Hilker & Richtler 2000; Pancino et al. 2000; van Leeuwen et al. 2000; Ferraro et al. 2004; Rey et al. 2004; Stanford et al. 2004, 2006; Sollima et al. 2005a; Villanova et al. 2007). These data, along with the apparent age dispersion at the main-sequence turnoff, suggest that ω Cen underwent extensive self-enrichment and star formation over >1 Gyr.

While ω Cen has an estimated mass of ∼(2–7) × $10^6 M_{\odot}$ (Richer et al. 1991; Meylan et al. 1995; van de Ven et al. 2006), it does not appear to have a particularly deep potential well compared to other lower mass clusters (Gnedin et al. 2002). Combined with the cluster's retrograde orbit and short disk crossing time (∼(1–2) × 10^8 yr; Dinescu et al. 1999), it seems unlikely that star formation could have occurred over several Gyr in the cluster's current configuration. A proposed scenario is that ω Cen was once the nucleus of a dwarf spheroidal galaxy that was accreted and stripped apart via gravitational interaction with the Milky Way (e.g., Bekki & Norris 2006). If this is true, then the cluster was probably much more massive in the past.

Until recently, ω Cen was the only known globular cluster with multiple populations, but new observations (e.g., Piotto 2008) have indicated several of the more massive clusters in the Galaxy host at least two SGBs and/or main sequences despite being monometallic. These anomalous sequences are often interpreted as having large He enhancements ranging from

[4] Visiting astronomer, Cerro Tololo Inter-American Observatory, National Optical Astronomy Observatory, which are operated by the Association of Universities for Research in Astronomy, under contract with the National Science Foundation.
[5] We make use of the standard spectroscopic notations where [A/B] ≡ $\log(N_A/N_B)_{star} - \log(N_A/N_B)_{\odot}$ and $\log \epsilon(A) \equiv \log(N_A/N_H)+12.0$ for elements A and B.

$Y \sim 0.30$–0.38, compared to the canonical He abundance of $Y \sim 0.25$. This assumption applies to the blue main sequence in ω Cen as well, which is roughly 0.3 dex more metal-rich than the red main sequence and requires $Y \sim 0.38$ to match the observations in this paradigm (Bedin et al. 2004; Norris 2004; Piotto et al. 2005). However, the important caveat remains that while the metallicity difference is *measured*, the He difference is only *inferred*. The source of these potential He enhancements remains unknown, but the most likely candidates include: 3–8 $M_{\odot}$ asymptotic giant branch (AGB) stars, super-AGB stars (∼8–10 $M_{\odot}$), massive rotating stars, and Population III stars (e.g., see Renzini 2008 for a review of this topic). Each of these scenarios poses a unique set of obstacles, but the basic problem is the difficulty in producing a discrete *population* of He-enriched stars while satisfying other chemical, age, and IMF constraints.

Globular cluster stars appear to have a more complex chemical history than their halo counterparts of similar metallicities, particularly with respect to the light elements oxygen through aluminum. In moderately metal-poor halo stars ($-2.0 \lesssim$ [Fe/H] $\lesssim -1.0$), these elements closely mimic the trends predicted for stars forming primarily out of gas polluted by core-collapse supernovae (SNe; e.g., Timmes et al. 1995; Samland 1998; Nomoto et al. 2006). That is, the α elements remain enhanced at [α/Fe] ∼ +0.40, but Na and Al, due to their secondary (i.e., metal-dependent) production, slowly increase relative to Fe with increasing metallicity. This is contrasted with the ubiquitous trends observed in globular clusters, which have stars with similar abundance patterns (the so-called primordial population) *and* stars showing signs of varying degrees of high-temperature proton-capture processing (the "intermediate" and "extreme" populations; e.g., Kraft 1994; Gratton et al. 2004; Carretta et al. 2008). These tell-tale signs of additional processing are evidenced by the pervasive O–Na and Mg–Al anticorrelations along with the Na–Al correlation observed in all well studied clusters to date, and are the result of processing in the ON, NeNa, and MgAl cycles (e.g., Gratton et al. 2004). Since these trends are observed in main sequence and turnoff stars (Cannon et al. 1998; Gratton et al. 2001; Cohen et al. 2002; Briley et al. 2004a, 2004b; Boesgaard et al. 2005) as well as RGB stars, it seems likely that the chemical patterns were already imprinted in the gas from which the current generation of stars formed. The source of these abundance patterns is unknown, but intermediate-mass AGB stars, which undergo hot bottom burning (HBB) at temperatures exceeding (80–100) × 10^6 K and experience third dredge-up, are a popular choice because they do not alter [Fe/H], have low-velocity ejecta, and produce large quantities of He, thus possibly alleviating some of the He enhancement issues mentioned above. While AGB stars are a qualitatively attractive solution, many problems arise in quantitative analyses and the ejecta yields are highly model dependent (e.g., Denissenkov & Herwig 2003; Fenner et al. 2004; Choi & Yi 2008; Ventura & D'Antona 2008). Other potential polluters include fast rotating massive stars (Decressin et al. 2007) and previous generations of slightly more massive RGB stars (Denissenkov & Weiss 2004); in situ deep mixing may also still play a role in highly evolved RGB stars.

In terms of chemical properties, ω Cen behaves similarly to Galactic globular cluster populations (aside from the large metallicity spread) in that the various light element relations and α enhancements are present in nearly all subpopulations analyzed so far (e.g., Norris & Da Costa 1995; Smith et al. 2000), but the cluster hosts stars of considerable Na/Al enrichment and O depletion. Unlike the field and disk populations that exhibit lower [α/Fe] ratios at [Fe/H] > −1, presumably due to the contributions of Type Ia SNe, the overwhelming majority of ω Cen stars at the same metallicity are α enhanced. This suggests that Type Ia SNe have played only a minor role in the cluster's chemical enrichment for all but perhaps the most metal-rich stars (Pancino et al. 2002; but see also Cunha et al. 2002). If ω Cen is the remnant of a former dwarf spheroidal galaxy then it has evolved much differently than present day dwarf galaxies because they do not show extreme light element enhancements/depletions and often exhibit subsolar [α/Fe] abundances (e.g., see review by Geisler et al. 2007). However, ω Cen does share the stronger *s*-process component seen in many dwarf spheroidal stars, except that the cluster stars more metal-rich than [Fe/H] ∼ −1.5 show *s*-/*r*-process ratios indicating complete *s*-process dominance whereas the dwarf galaxies experienced much weaker *s*-process enrichment. This is in direct contradiction to globular clusters, which are *r*-process rich. Lower mass AGB stars (∼1–4 $M_{\odot}$), which are thought to produce most of the *s*-process elements, have therefore had a much more significant effect on ω Cen's chemical evolution than is seen in dwarf spheroidals and globular clusters.

In this paper, we present spectroscopic analyses of numerous light, α, Fe-peak, and neutron-capture elements for 66 stars spanning ω Cen's full metallicity range, with an emphasis on the lesser studied intermediate and metal-rich populations. We combine our results with those from the literature and compare ω Cen to the Galactic thin and thick disk, halo, bulge, other globular clusters, and nearby dwarf spheroidals in an attempt to disentangle the evolution of these very different populations and perhaps isolate chemical signatures that are unique to each subpopulation in ω Cen.

2. OBSERVATIONS AND REDUCTIONS

All observations were taken at the Cerro Tololo Inter-American Observatory on 2006 May 26 and 2006 May 27 using the Blanco 4 m telescope and Hydra multifiber spectrograph. In each configuration, we used the "large" 300 μm (2″) fibers and obtained spectra with two different bench spectrograph setups. The first setup was centered near 6670 Å and spanned approximately 6530–6800 Å while the second setup was centered on 6125 Å and ranged from 6000–6250 Å. Both spectrograph setups employed the 100 μm slit mask along with the 400 mm Bench Schmidt Camera and 316 line mm^{-1} echelle grating to achieve a resolving power of $R(\lambda/\Delta\lambda) \approx 18{,}000$ (0.35 Å FWHM).

Target stars, coordinates, photometry, and membership probabilities were taken from the proper motion study by van Leeuwen et al. (2000). The targets were chosen to be on the upper third of the giant branch and all have $V < 14.0$, but priority was given to those with larger $B - V$ indices (i.e., more metal-rich) in the Hydra assignment code. Stars with membership probabilities <70% were excluded from the fiber assignment process. While we did not measure radial velocities for the target stars, cluster members were easily discerned from the field star population because of ω Cen's comparatively large radial velocity ($\langle V_R \rangle \sim 232$ km s^{-1}; Reijns et al. 2006).

We obtained three, 1800 s exposures for each spectrograph setup with 92 fibers placed on targets. The co-added signal-to-noise ratios (S/N) of the spectra ranged from ∼25 to 200, but we only analyzed stars for which the S/N was $\gtrsim$50. The final sample includes 66 stars and is shown in Figure 1 along with

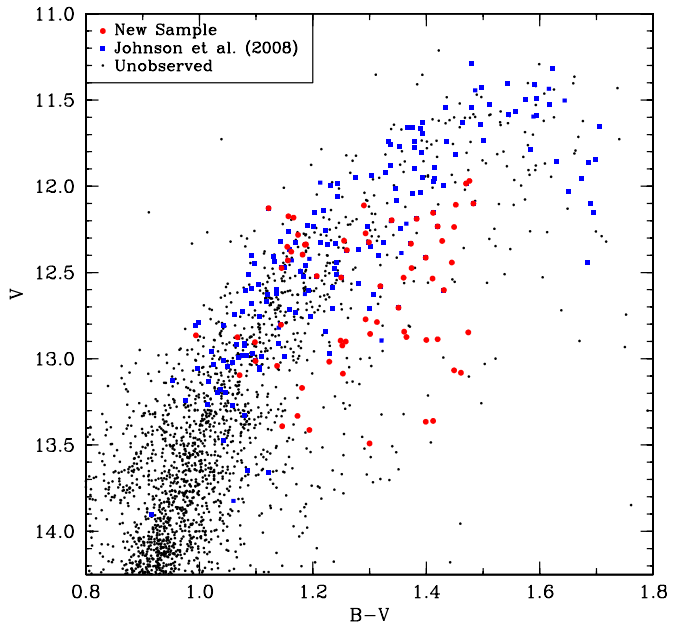

Figure 1. Color–magnitude diagram of ω Cen's RGB. The filled red circles represent the stars observed for this study and the filled blue squares show the stars observed for Johnson et al. (2008). There are 22 stars which overlap with Johnson et al. and those are also indicated by filled red circles. The complete sample, including stars not observed here, are from van Leeuwen et al. (2000).

(A color version of this figure is available in the online journal.)

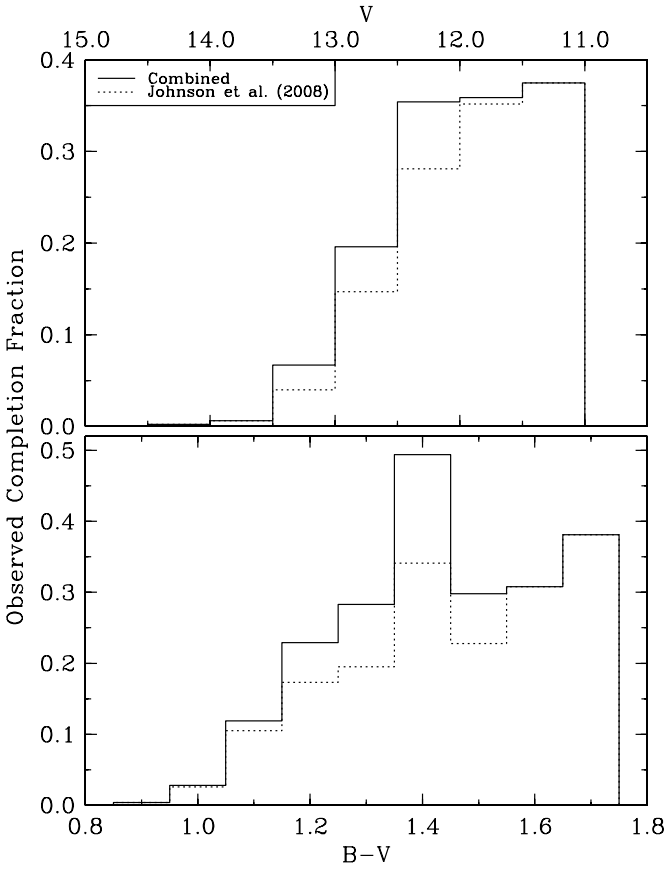

Figure 2. Histogram showing the observed completion fraction of this study combined with the data of Johnson et al. (2008). The top panel shows the completion fraction as a function of V magnitude and the bottom panel shows the completion fraction as a function of $B-V$ color.

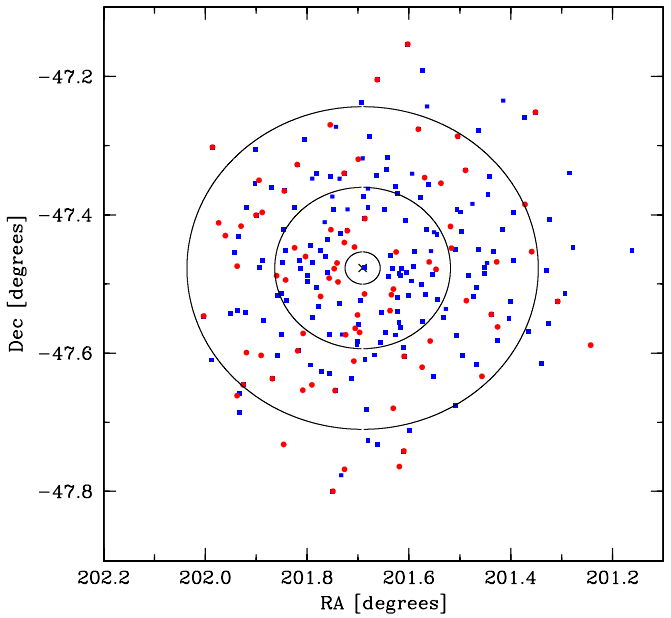

Figure 3. Program stars are shown in terms of position in the field. The symbols are the same as in Figure 1. The cross indicates the field center at 201.°691, −47.°4769 (J2000) ($13^h26^m45^s.9$, −47°28′37.″0) and the ellipses indicate 1, 5, and 10 times the core radius of 1.′40.

(A color version of this figure is available in the online journal.)

the data from Johnson et al. (2008) and the full sample of van Leeuwen et al. (2000).

Since ω Cen exhibits such a large range in metallicity and the various giant branches contain stars in different ratios, selection effects may be more prominent than for typical globular clusters. In Figure 2, we show the observed completion fractions of our current data combined with Johnson et al. (2008) as a function of both V magnitude and $B-V$ color. While there was little increase in the completion fraction for stars with $11.0 < V < 12.0$, those with $12.0 < V < 13.5$ increased ∼5%–10% and similar additions are seen in $B-V$ ranging from 1.15 to 1.55. We now have data that are at least uniformly representative across a wide range of temperatures and luminosities; however, the sample is still weighted toward observing more stars in the most metal-poor population. Since the new observations preferentially target stars with metallicities in the range $-1.50 \lesssim$ [Fe/H] $\lesssim -0.50$, the increased H^- opacity and line blocking with increasing metallicity causes these stars to have lower flux in the spectral regions of interest than their more metal-poor counterparts. As a result, stars observed in progressively more metal-rich branches are, on average, more evolved with our magnitude cutoff.

There is some evidence for the presence of a radial metallicity gradient in the cluster (Norris et al. 1996, 1997; Suntzeff & Kraft 1996; Hilker & Richtler 2000; Pancino et al. 2000; Rey et al. 2004; Johnson et al. 2008), and it is important to observe stars at various radii to measure the true metallicity distribution. In Figures 3 and 4, we plot the positions of our program stars and show a normalized cumulative distribution as a function of distance from the cluster center, defined by van Leeuwen et al. (2000) as $13^h26^m45^s.9$, –47°28′37.″0 (J2000). Both figures indicate our combined sample from this study and Johnson et al. (2008) mostly covers stars between ∼5′ and 15′ from the center, which is equivalent to roughly 3.5–10.5 core radii where the core radius is 1.′40 (Harris 1996; rev. 2003 February). Fiber positioning limitations and increasing stellar densities near the cluster core prevent us from obtaining copious observations

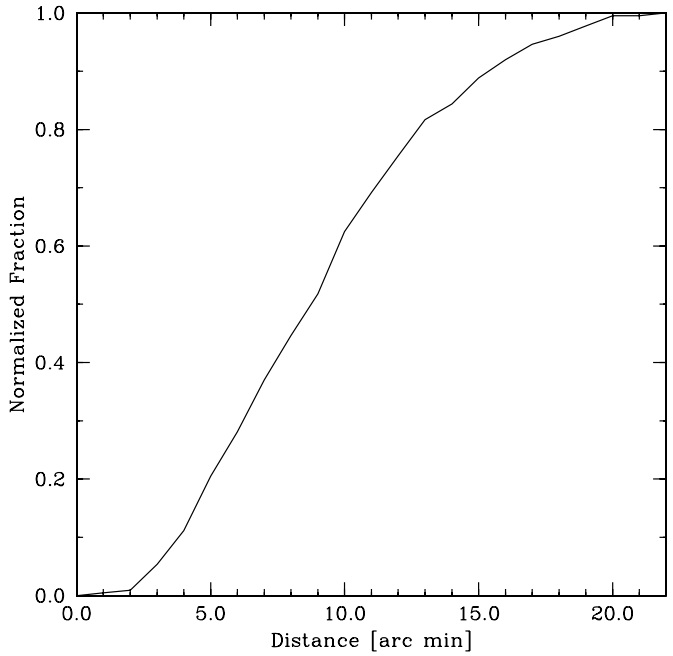

Figure 4. Normalized cumulative distribution for our combined sample as a function of distance from the cluster center. This plot shows the fraction of our total sample observed inside a given radius. The cluster center reference is the same as in Figure 3.

inside ∼1′–2′ from the center, but we have observed nearly 30%–40% of all bright giants inside 10′–20′.

Data reductions were carried out using various tasks provided in standard IRAF[6] packages. We used *ccdproc* to trim the overscan region and apply the bias level corrections. Flat-field corrections, ThAr lamp wavelength calibrations, cosmic ray removal, subtraction of scattered light and sky spectra, and extraction of the one-dimensional spectra were performed using the *dohydra* package. The resultant spectra were then corrected for telluric contamination, continuum flattened, and combined.

3. ANALYSIS

We have derived abundances for nine different elements using local thermodynamic equilibrium (LTE) equivalent width and spectrum synthesis analyses in the combined spectral regions of 6000–6250 Å and 6530–6800 Å. Spectrum synthesis was used for determining all Al abundances because of the potential for CN contamination in metal-rich and CN-strong stars. Model atmosphere parameters including effective temperatures ($T_{\rm eff}$), surface gravities (log g), and microturbulence ($V_{\rm t}$) were estimated based on published photometry and the empirical $V_{\rm t}$–$T_{\rm eff}$ relation given in Johnson et al. (2008).

3.1. Model Stellar Atmospheres

Effective temperatures were estimated via empirical calibrations of V and Two Micron All Sky Survey (2MASS) photometry based on the infrared flux method (Blackwell & Shallis 1977). To improve accuracy, we averaged the $T_{\rm eff}$ values obtained through the color–temperature relations of Alonso et al. (1999, 2001) and Ramírez & Meléndez (2005) for $V-J$, $V-H$, and $V-K$ color indices. The photometry was corrected for interstellar reddening and extinction using the corrections recommended by Harris (1996) of $E(B-V) = 0.12$ and McCall (2004) for $E(V-J)/E(B-V) = 2.25$, $E(V-H)/E(B-V) = 2.55$, and $E(V-K)/E(B-V) = 2.70$. Evidence for differential reddening is mainly concentrated near the core (Calamida et al. 2005; van Loon et al. 2007), but the well defined evolutionary sequences seen in Villanova et al. (2007) suggest that significant differential reddening is unlikely. Therefore, we have applied a uniform reddening correction to all stars. The temperatures derived from each color index are in very good agreement with an average offset of 21 K ($\sigma = 6$ K). Our adopted $T_{\rm eff}$ values are probably accurate to within ±50 K, and are consistent with the star-to-star scatter seen in the calibrations of both studies. Plotting Fe abundance versus excitation potential did not reveal any trends and our adopted photometric temperatures satisfied excitation equilibrium.

Surface gravity was determined by $T_{\rm eff}$ and absolute bolometric magnitude ($M_{\rm bol}$) through the standard relation,

$$\log(g_*) = 0.40(M_{\rm bol.} - M_{\rm bol.\odot}) + \log(g_\odot) + 4(\log(T/T_\odot)) + \log(M/M_\odot). \quad (1)$$

We applied the bolometric correction to $M_{\rm V}$ from Alonso et al. (1999) and used a distance modulus of $(m-M)_{\rm V} = 13.7$ (van de Ven et al. 2006). As mentioned in Section 1, an age spread of ∼1–4 Gyr is likely present in the cluster, but the difference in mass between the oldest and youngest stars is only of the order of ∼0.05 $M_\odot$, which is negligible for surface gravity determinations. Norris et al. (1996) argue that 20%–40% of stars on the RGB may be AGB stars with $M \sim 0.60\ M_\odot$, but this would only lead to abundance uncertainties of the order of 0.10 dex for species residing in the dominant ionization state (e.g., Fe II). Similar surface gravity and abundance effects may be expected for He-rich stars, which have slightly lower RGB masses due to their shorter lifetimes compared to He-normal stars (e.g., Newsham & Terndrup 2007).

Since we only had a limited number of singly ionized lines available for analysis relative to the number of neutral lines, we relied on the photometric surface gravity estimate instead of ionization equilibrium. In the top panel of Figure 5, we show the differences in derived abundance for neutral and singly ionized species of Fe, Sc, and Ti. For Fe, the average offset between log ϵ(Fe I) and log ϵ(Fe II) is −0.09 ($\sigma = 0.12$), but this is based on a highly discrepant number of lines between the two species and thus may not accurately reflect a systematically low gravity. Sc shares a similar pattern with an average difference of −0.16 dex ($\sigma = 0.22$), but these are based on only one line a piece for each species and reliable hyperfine structure information for these transitions is sparse. Ti I and II lines give an average difference of −0.01 dex ($\sigma = 0.18$). Overall, the difference between abundances derived from both species is −0.07 dex ($\sigma = 0.17$), which is comparable to measurement and model uncertainties. In the bottom panel of Figure 5, we show photometric log g values compared with estimates based on spectroscopic gravity calibrations of globular clusters provided by Kučinskas et al. (2006). The average offset between the two systems is +0.04 dex ($\sigma = 0.17$), and is comparable to the uncertainty found by examining ionization equilibrium. This leads us to believe that our surface gravity estimates are not in serious error.

We obtained a rough estimate of [Fe/H] using the [Ca/H] calibration based on V and $B-V$ given in van Leeuwen et al. (2000; their Equation (15)) and assumed [Ca/Fe] ∼ +0.30. Likewise, an initial microturbulence value was calculated from

[6] IRAF is distributed by the National Optical Astronomy Observatories, which are operated by the Association of Universities for Research in Astronomy, Inc., under cooperative agreement with the National Science Foundation.

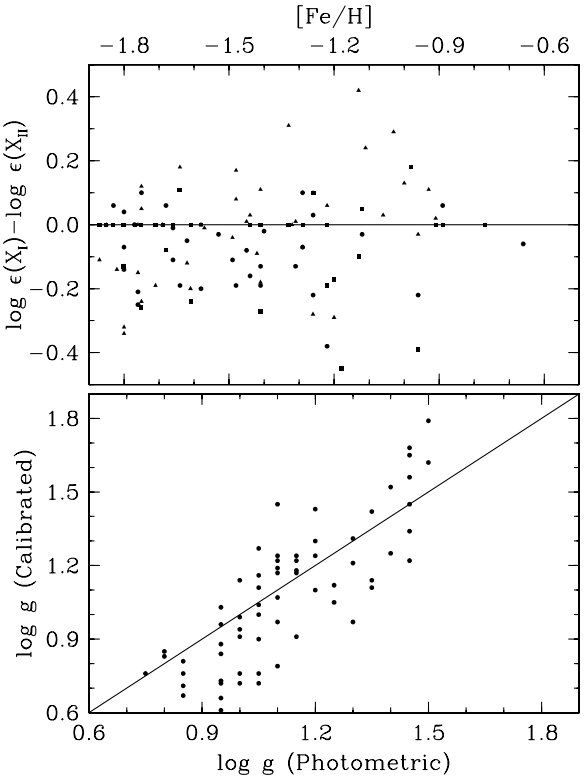

Figure 5. Top panel shows a plot of the difference in abundance as derived from both neutral and singly ionized species as a function of [Fe/H]. The filled circles represent Fe, the filled boxes are Sc, and the filled triangles are Ti. The bottom panel shows the log g values adopted from photometry versus the calibrated $T_{\rm eff}$–log g relation from Kučinskas et al. (2006). In both panels the straight line indicates perfect agreement.

the $V_{\rm t}$–$T_{\rm eff}$ relation given in Johnson et al. (2008) for luminous giants. Our determined $T_{\rm eff}$, log g, [Fe/H], and $V_{\rm t}$ values were used to generate model atmospheres (without convective overshoot) via interpolation within the ATLAS9[7] grid (Castelli et al. 1997). We iteratively adjusted the microturbulence of the model until Fe abundances were independent of line strength following the method described in Magain (1984). Lastly, the model's metallicity was adjusted to match the derived Fe abundance of each star. A complete list of our adopted model atmosphere parameters along with star identifiers, published photometry, membership probabilities, and S/N estimates for each spectrum are provided in Table 1.

3.2. Derivation of Abundances

3.2.1. Equivalent Width Analysis

For all elements except Al, final abundances were determined using equivalent width analyses and the *abfind* driver in the LTE line analysis code MOOG (Sneden 1973). Equivalent widths were measured by interactively fitting multiple Gaussians to isolated and blended line profiles. Suitable lines were identified using the solar and Arcturus atlases.[8] Our adopted log gf values were determined by measuring equivalent widths in the solar atlas and then modified until all lines yielded abundances consistent with the photospheric values given in Anders & Grevesse (1989). A summary of our line list and measured equivalent widths is given in Table 2 and the final abundances are in Table 3. Note that all abundance ratios in Table 3 are relative to $[{\rm Fe/H}]_{\rm avg.}$, which is the average of [Fe I/H] and [Fe II/H] or just [Fe I/H] if Fe II lines are not available. We did not determine [X/Fe] ratios by matching ionization states because many stars did not have reliable Fe II transitions, our typical measured [Fe I/H] values are based on more than 25 lines versus 1 or 2 for [Fe II/H], and ⟨[Fe I/H]–[Fe II/H]⟩ is approximately equal to the line-to-line dispersion seen in our [Fe I/H] determinations. Giving [X/Fe] ratios relative to $[{\rm Fe/H}]_{\rm avg.}$ is an attempt to minimize the effects of overionization.

Many line profiles for the odd-Z Fe-peak and neutron-capture elements suffer from hyperfine splitting, but the necessary atomic data for several of these transitions are not currently available in the literature. A standard equivalent width analysis will produce an overabundance if this effect is not properly taken into account. Since the error caused by hyperfine splitting increases with line strength, we do not expect our abundances, which are based on unsaturated and generally weak lines, to be strongly affected.

The elements here that may be affected by hyperfine splitting are Sc, La, and Eu. Our Sc abundances are based on the 6210.67 Å Sc I line and 6604.60 Å Sc II line. While hyperfine structure estimates have been produced for Sc II (Prochaska & McWilliam 2000), there is no available information for the Sc I line and neither of these transitions is included in Zhang et al. (2008). Therefore, we have not applied the correction to Sc II, but the offset is probably not too large given that the average equivalent width for the Sc I/II lines is ∼60 mÅ. Similarly, no hyperfine data exist for the 6774.27 Å La II line and therefore we accept the derived abundances at face value. Europium is slightly more complicated because, in addition to hyperfine splitting, it has two stable, naturally occurring isotopes (^{151}Eu and ^{153}Eu) that are present in nearly equal proportions. For all Eu abundances, we have applied a hyperfine and isotopic line list provided by C. Sneden (2006, private communication). Lacking a priori knowledge of the r-/s-process contributions for La and Eu in ω Cen, we have assumed a solar mix such that the ratio for La is 25%/75% (Sneden et al. 2008) and for Eu 97%/3% (Sneden et al. 1996), respectively.

3.2.2. Spectrum Synthesis Analysis

While all other abundances were determined using equivalent width analyses, we derived Al abundances via spectrum synthesis because of the nontrivial contamination from CN lines seen in many of the cooler, more metal-rich stars. For consistency, spectrum synthesis was performed even in cases where CN contamination was not an issue. In Figure 6, we show two sample syntheses for a case with strong (top panel) and weak (bottom panel) CN lines in order to illustrate the line blanketing effects from molecular absorption. For stars where the CN lines were present, we found that a straightforward equivalent width analysis led to an overestimate of log ϵ(Al) by as much as 0.1–0.2 dex compared to spectrum synthesis, but the two methods agreed to within <0.1 dex in spectra without strong CN features. The Al lines are designated by "synth" in Table 2.

We created the molecular line list by combining the Kurucz online database[9] with one provided by B. Plez (2007, private communication; see also Hill et al. 2002). Since the C, N, and ^{12}C/^{13}C abundances are unknown, we fixed [C/Fe] = −0.5

[7] The model atmosphere grids can be downloaded from http://cfaku5.cfa.harvard.edu/grids.html.

[8] The atlases can be downloaded from the NOAO Digital Library at http://www.noao.edu/dpp/library.html.

[9] The Kurucz line lists can be accessed at http://kurucz.harvard.edu/linelists.html.

Table 1
Photometry, Membership, and Model Atmosphere Parameters

Star LEID[a]	Alt. ROA[b]	V	$B-V$	J	H	K	M_V^0	Mem. Prob.[c]	$T_{\rm eff}$ (K)	log g (cm s^{-2})	[Fe/H] Avg.	V_t (km s^{-1})	S/N 6125 Å	S/N 6670 Å
9	370	12.529	1.250	10.382	9.755	9.627	−1.543	99	4505	1.20	−1.41	2.05	100	100
6017	240	12.233	1.420	9.717	8.982	8.808	−1.839	98	4145	0.85	−1.22	2.00	125	100
12013	394	12.579	1.319	10.242	9.560	9.402	−1.493	98	4305	1.10	−1.31	1.85	100	125
15023	234	12.182	1.166	9.964	9.352	9.231	−1.890	100	4455	1.05	−1.80	2.05	125	150
16015	213	12.127	1.122	9.979	9.373	9.210	−1.945	100	4510	1.05	−1.80	1.60	125	125
17015	325	12.430	1.156	10.235	9.610	9.497	−1.642	100	4470	1.15	−1.82	1.65	150	100
19062	464	12.803	1.144	10.601	10.001	9.872	−1.269	98	4470	1.30	−1.75	1.50	100	100
22037	307	12.339	1.186	10.178	9.559	9.402	−1.733	100	4485	1.10	−1.76	1.90	150	150
23061	296	12.337	1.188	10.158	9.472	9.390	−1.735	100	4460	1.10	−1.66	1.65	150	125
24027	5969	13.013	1.099	10.952	10.344	10.226	−1.059	100	4600	1.45	−1.57	1.80	125	75

Notes.
[a] Identifier from van Leeuwen et al. (2000).
[b] Identifier from Woolley (1966).
[c] Membership probability from van Leeuwen et al. (2000).

(This table is available in its entirety in a machine-readable form in the online journal. A portion is shown here for guidance regarding its form and content.)

Table 2
Linelist and Equivalent Widths

λ (Å)	Element	E.P. (eV)	log gf	9	6017	12013	15023	16015	17015	19062	22037	23061	24027	24056
6003.01	Fe I	3.88	−1.07	···	···	···	···	···	···	···	40	···	···	46
6007.32	Ni I	1.68	−3.35	···	70	···	···	···	···	···	21	···	···	22
6007.97	Fe I	4.65	−0.70	···	53	···	···	···	···	···	···	···	19	···
6008.57	Fe I	3.88	−0.94	···	99	···	···	···	···	···	···	···	···	···
6015.25	Fe I	2.22	−4.66	···	17	12	···	···	···	···	···	···	···	···
6024.07	Fe I	4.55	−0.06	84	107	89	59	52	59	61	58	60	···	49
6027.06	Fe I	4.07	−1.14	47	68	63	25	15	24	35	22	28	57	20
6035.35	Fe I	4.29	−2.56	···	···	···	···	···	···	···	···	···	···	···
6056.01	Fe I	4.73	−0.44	52	51	43	23	22	18	36	16	26	30	···
6064.63	Ti I	1.05	−1.92	22	60	59	12	···	8	21	7	11	8	8

(This table is available in its entirety in a machine-readable form in the online journal. A portion is shown here for guidance regarding its form and content.)

Table 3
Derived Abundances

Star LEID	[Fe I/H]	[Fe II/H]	[Fe/H] Avg.	[Na I/Fe]	[Al I/Fe]	[Ca I/Fe]	[Sc I/Fe]	[Sc II/Fe]	[Sc/Fe] Avg.	[Ti I/Fe]	[Ti II/Fe]	[Ti/Fe] Avg.	[Ni I/Fe]	[La II/Fe]	[Eu II/Fe]
9	−1.47	−1.34	−1.41	−0.08	+0.06	+0.26	−0.07	+0.21	+0.07	+0.08	−0.03	+0.03	−0.06	−0.41	−0.41
6017	−1.41	−1.03	−1.22	+0.36	+1.01	+0.20	···	···	···	−0.07	−0.13	−0.10	−0.21	+0.89	−0.16
12013	−1.37	−1.24	−1.31	+0.36	+0.24	+0.40	−0.10	···	−0.10	+0.21	+0.20	+0.21	−0.03	+0.29	−0.46
15023	−1.87	−1.73	−1.80	−0.50	+0.18	+0.20	···	+0.12	+0.12	+0.04	+0.38	+0.21	−0.04	−0.03	−0.21
16015	−1.83	−1.76	−1.80	−0.66	+0.13	+0.30	···	···	···	+0.16	+0.30	+0.23	−0.10	+0.15	+0.18
17015	−1.82	···	−1.82	···	···	+0.38	···	+0.39	+0.39	+0.09	+0.23	+0.16	−0.07	−0.07	+0.02
19062	−1.70	−1.80	−1.75	+0.07	···	+0.46	+0.27	···	+0.27	+0.21	+0.45	+0.33	+0.04	+0.58	+0.27
22037	−1.88	−1.63	−1.76	−0.09	+0.82	+0.23	···	+0.11	+0.11	+0.07	+0.23	+0.15	−0.11	−0.40	+0.30
23061	−1.71	−1.60	−1.66	−0.29	···	+0.24	···	···	···	+0.08	···	+0.08	−0.17	−0.29	+0.11
24027	−1.57	···	−1.57	+0.43	+1.18	+0.44	···	+0.18	+0.18	+0.23	+0.24	+0.23	+0.03	+0.36	+0.25

(This table is available in its entirety in a machine-readable form in the online journal. A portion is shown here for guidance regarding its form and content.)

and $^{12}C/^{13}C = 4$, which are consistent with Norris & Da Costa (1995) and Smith et al. (2002) for ω Cen giants. Without accurate C, N, and O data, it is impossible to constrain the molecular equilibrium equations and derive true C and/or N abundances for CN. Therefore, we treated the nitrogen abundance as a free parameter and adjusted it to obtain a best fit to the CN lines. Other metal lines surrounding the Al doublet have excitation potentials $\gtrsim$5 eV and are not important contributors in these cool stars.

3.2.3. Abundance Comparison to Other Studies

Although ω Cen has been the subject of many spectroscopic studies, here we restrict comparison to those measuring abundances using moderately high resolution ($R \gtrsim 15{,}000$) spectroscopy. The only two previous works for which we have several stars in common are Norris & Da Costa (1995) and Johnson et al. (2008). In the case of Norris and Da Costa, the average difference in measured [Fe/H] for the seven common stars is

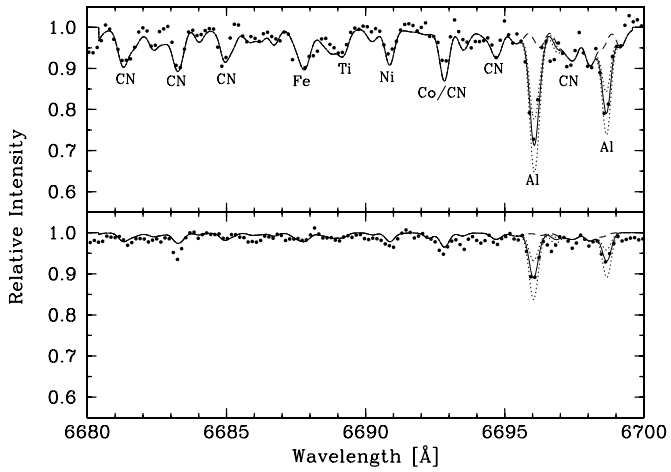

Figure 6. Sample spectrum syntheses are shown for two stars of varying $T_{\rm eff}$, [Fe/H], and CN strength, but similar [Al/Fe] ratios. The relative intensity scales are the same in both figures. The solid line shows the best fit to the observed spectrum, the dotted lines illustrate deviations ±0.30 dex, and the dashed line indicates how the spectrum would appear if Al were absent.

−0.02 dex ($\sigma = 0.05$), in the sense present minus Norris and Da Costa. The results are similar for most of the other elements with average differences of the order of ±0.10 dex ($\sigma \sim 0.15$), and La is the only exception with an average offset of +0.34 ($\sigma = 0.12$). This discrepancy is likely due to the difficulty in obtaining accurate La abundances. In comparison to Johnson et al. (2008), the difference in [Fe/H] based on 21 stars in common is −0.10 dex ($\sigma = 0.05$) and 0.00 dex ($\sigma = 0.22$) for [Al/Fe]. These results are consistent with the small deviations in adopted atmospheric parameters found by Johnson et al. (2008; see their Figures 8–9) comparing that study to other spectroscopic surveys in the literature.

3.3. Abundance Sensitivity to Model Atmosphere Parameters

In Table 4, we show the results of our tests regarding abundance sensitivity to uncertainties in adopted model atmosphere parameters for all elements studied here. We examined how the various log ϵ(X) values changed when altering $T_{\rm eff}$ ± 100 K, log g ± 0.30 cm s^{-2}, [M/H] ± 0.30 dex, and $V_{\rm t}$ ± 0.30 km s^{-1}. In general, we find that the neutral species tend to be more strongly affected by changes in temperature, but the singly ionized species are influenced by surface gravity changes because of their dependence on electron pressure. However, abundances taken from singly ionized transitions tend to have a larger dependence on $T_{\rm eff}$ with increasing metallicity while the effects on neutral lines are mitigated. Similarly, only the ionized species have a significant dependence on the model atmosphere's overall metallicity because their line-to-continuous opacity ratios are more sensitive to changes in the H$^-$ abundance. For stars with [Fe/H] $\lesssim -1$, microturbulence uncertainties have very little influence on the derived abundance because the lines are weak and lie further down the linear portion of the curve of growth, but even in the most metal-rich stars the effects are typically no larger than ±0.10–0.15 dex. The lanthanum line is an exception because the more metal-rich ω Cen stars are very *s*-process-rich and thus the La II lines typically have equivalent widths $\gtrsim$75 m Å. Although each element has a slightly different dependence on these physical parameters, the important point is that the element-to-iron ratio should be mostly invariant. Instead, only the log ϵ(X) values should be sensitive to model parameter variations.

Table 4
Abundance Sensitivity to Model Atmosphere Parameters

Element	$\Delta T_{\rm eff}$ ± 100 (K)	Δlog g ± 0.30 (cm s^{-2})	Δ[M/H] ± 0.30 (dex)	$\Delta V_{\rm t}$ ± 0.30 (km s^{-1})
		[Fe/H] ≈ −2.0		
Fe I	±0.14	∓0.01	∓0.04	∓0.06
Fe II	∓0.02	±0.11	±0.06	∓0.01
Na I	±0.08	∓0.03	∓0.03	±0.00
Al I	±0.07	∓0.02	∓0.03	∓0.02
Ca I	±0.12	∓0.04	∓0.06	∓0.10
Ti I	±0.19	∓0.03	∓0.05	∓0.01
Ti II	∓0.04	±0.12	±0.08	∓0.03
Sc I	±0.21	∓0.01	∓0.06	±0.00
Sc II	±0.02	±0.11	±0.07	∓0.04
Ni I	±0.14	±0.01	∓0.03	∓0.04
La II	±0.05	±0.12	±0.08	±0.00
Eu II	±0.01	±0.11	±0.07	±0.00
		[Fe/H] ≈ −1.5		
Fe I	±0.09	±0.04	±0.01	∓0.08
Fe II	∓0.06	±0.15	±0.08	∓0.01
Na I	±0.09	∓0.02	∓0.02	∓0.01
Al I	±0.08	∓0.01	∓0.02	∓0.01
Ca I	±0.14	∓0.03	∓0.04	∓0.15
Ti I	±0.19	±0.00	∓0.04	∓0.04
Ti II	∓0.05	±0.13	±0.09	∓0.03
Sc I	±0.24	±0.01	∓0.02	∓0.01
Sc II	∓0.02	±0.13	±0.10	∓0.06
Ni I	±0.05	±0.05	±0.03	∓0.06
La II	±0.03	±0.13	±0.10	∓0.03
Eu II	∓0.02	±0.13	±0.10	±0.00
		[Fe/H] ≈ −1.0		
Fe I	±0.08	±0.06	±0.02	∓0.11
Fe II	∓0.13	±0.18	±0.11	∓0.03
Na I	±0.11	∓0.01	∓0.04	∓0.08
Al I	±0.10	±0.00	∓0.03	∓0.08
Ca I	±0.15	∓0.04	∓0.02	∓0.17
Ti I	±0.19	±0.00	∓0.04	∓0.08
Ti II	∓0.05	±0.14	±0.10	∓0.13
Sc I	±0.24	±0.01	∓0.03	∓0.04
Sc II	∓0.02	±0.14	±0.11	∓0.04
Ni I	±0.04	±0.07	±0.05	∓0.09
La II	±0.05	±0.14	±0.09	∓0.19
Eu II	∓0.02	±0.13	±0.11	∓0.01
		[Fe/H] ≈ −0.5		
Fe I	±0.02	±0.05	±0.07	∓0.14
Fe II	∓0.19	±0.14	±0.17	∓0.04
Na I	±0.10	∓0.04	±0.00	∓0.13
Al I	±0.09	∓0.01	∓0.01	∓0.10
Ca I	±0.14	∓0.06	±0.02	∓0.15
Ti I	±0.16	±0.02	∓0.01	∓0.16
Ti II	±0.06	±0.15	±0.11	±0.14
Sc I	±0.21	±0.04	∓0.02	∓0.14
Sc II	±0.02	±0.16	±0.13	±0.05
Ni I	±0.00	±0.08	±0.09	∓0.11
La II	±0.03	±0.11	±0.12	∓0.26
Eu II	∓0.02	±0.12	±0.12	∓0.01

As mentioned in Section 1, it has been argued that several of the intermediate and perhaps metal-rich stars in this cluster may have strong He enhancements extending as large as $Y \sim 0.38$. We do not expect our analysis to be severely altered (see Girardi et al. 2007) and the [X/Fe] ratios should be mostly independent of the adopted He abundance; however, [Fe/H] may be systematically higher in the He-rich stars. To test the effects of He enhancement, we created synthetic spectra using

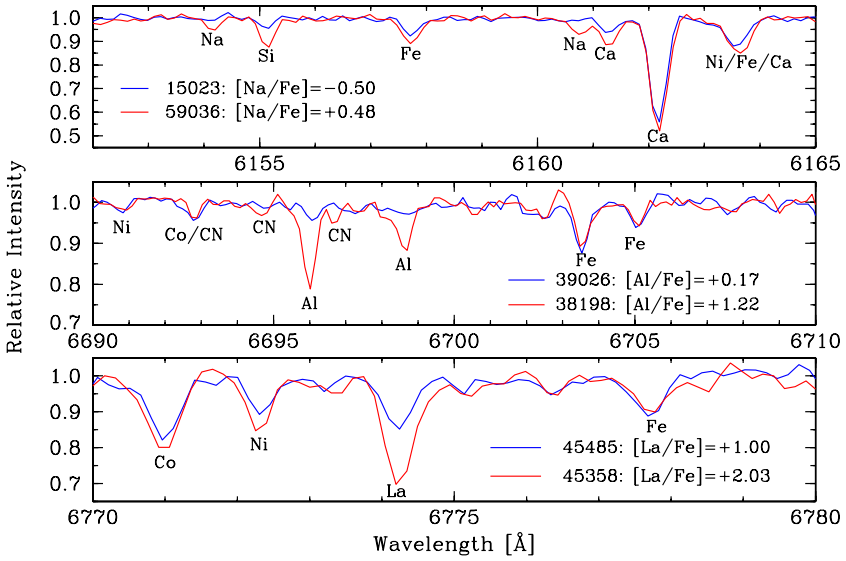

Figure 7. Sample spectra are shown in three different wavelength regions to highlight the line strength differences seen in Na, Al, and La. Each panel contains stars of roughly the same $T_{\rm eff}$ and [Fe/H]. Note the differences seen in both the Si and Ca features compared to Fe in the top panel.

(A color version of this figure is available in the online journal.)

He-normal ($Y = 0.27$) and He-rich ($Y = 0.35$) ATLAS9 models of comparable temperature and metallicity to our stars. We found the line strength differences between the two sets to be much less than 1%, with the He-rich model producing stronger lines because of decreased continuous H^- opacity. This result is consistent with Piotto et al. (2005) and leads us to believe that our abundances are robust against possible He variations.

4. RESULTS

4.1. Light Elements: Na and Al

The odd-Z elements Na and Al are particularly important because they are among the heaviest elements thought to be produced via proton-capture nucleosynthesis in low- and intermediate-mass stars. This makes them useful probes for deciphering which processes, in addition to Type II SN production, may have been dominant during various epochs of star formation. Previous large sample, high-resolution spectroscopic studies of ω Cen giants (e.g., Norris & Da Costa 1995; Smith et al. 2000; Johnson et al. 2008) have shown that Na and Al (in addition to C, N, O, and Mg) exhibit very large star-to-star [X/Fe] variations while preserving the Na–Al correlation seen in other Galactic globular clusters. The top two panels of Figure 7 illustrate this point by demonstrating the stark contrast in Na and Al line strengths for stars with similar temperatures and metallicities. Since we can compare stars of similar evolutionary state and metallicity, we can safely assume that departures from LTE are not the cause of the observed abundance variations. No NLTE corrections have been applied to our Na and Al results because there are no "standard" values available in the literature and those that are available disagree in magnitude and sign. However, Na and Al abundances determined from the nonresonance, subordinate transitions used here typically have corrections of the order of $\lesssim$0.20 dex for stars with –2.5 < [Fe/H] < −0.5 (e.g., Gratton et al. 1999; Gehren et al. 2004).

First considering our Na results, we find that there is a general increase in ⟨[Na/Fe]⟩ as a function of increasing metallicity accompanied by a decrease in the star-to-star scatter. The dominant metallicity group of stars ($-1.8 \lesssim$ [Fe/H] $\lesssim -1.6$) have ⟨[Na/Fe]⟩ = +0.03 (σ = 0.32) with a full range of 1.29 dex while the next population of stars ($-1.5 \lesssim$ [Fe/H] $\lesssim -1.3$) have ⟨[Na/Fe]⟩ = +0.20 (σ = 0.21) and a full range of 0.67 dex, which is smaller by about a factor of 4. However, there is a noticeable change in the distribution of [Na/Fe] for RGB stars in the higher metallicity populations. At [Fe/H] $\gtrsim -1.2$, 95% (18/19) of the stars are very Na-rich with ⟨[Na/Fe]⟩ = +0.86 (σ = 0.12). The strong enrichment of this population is in agreement with Norris & Da Costa (1995) who find that at least 75% (6/8) of stars in that metallicity range are Na-rich and at least 50% are O-poor. A two-sample Kolmogorov–Smirnov (K–S) test (Press et al. 1992) shows that the population of stars with [Fe/H] < −1.2 is drawn from a different parent population than the [Fe/H] < −1.2 group at the 99% level.

By combining our current data with that of Johnson et al. (2008), we have a homogeneous set of [Al/Fe] abundances determined for more than 200 RGB stars. In Figure 8, we show the results of our combined samples for [Al/Fe] and log ϵ(Al) as a function of metallicity. Although the sample sizes between Na and Al differ by a factor of 3.5, some key differences standout in the Al data set: (1) there appear to be two or three different populations of stars, (2) the star-to-star dispersion stays mostly constant until [Fe/H] ∼ −1.2, and (3) stars with [Fe/H] $\gtrsim -1.2$ show a roughly constant log ϵ(Al) ≈ 6.22 (σ = 0.18) as a function of increasing [Fe/H]. However, there are some interesting similarities: (1) the Al data show a clear change in the abundance pattern for stars with [Fe/H] $\gtrsim -1.2$, (2) the metal-rich RGB stars are predominantly Al-rich, and (3) log $\epsilon(\mathrm{Na})_{\rm max} \approx$ log $\epsilon(\mathrm{Al})_{\rm max}$. It should be noted that despite the large abundance scatter, the Na–Al correlation is present in our data.

We define the three different Al populations as those having [Al/Fe] < +0.60, +0.60 ⩽ [Al/Fe] < +1.0, and [Al/Fe] ⩾ +1.0. First considering only stars with [Fe/H] < −1.2, the subpopulations break down into ⟨[Al/Fe]⟩ = +0.34 (σ = 0.14), ⟨[Al/Fe]⟩ = +0.82 (σ = 0.10), and ⟨[Al/Fe]⟩ = +1.17 (σ = 0.11), respectively. These represent 50% (83/166), 30% (49/

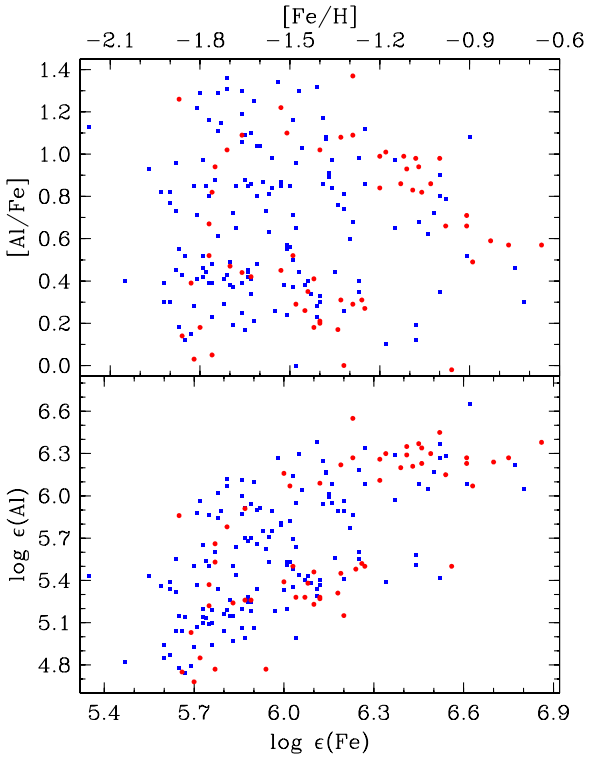

Figure 8. Top panel shows [Al/Fe] plotted as a function of [Fe/H] and the bottom panel shows log ϵ(Al) plotted as a function of log ϵ(Fe). The symbols are the same as those in Figure 1.

(A color version of this figure is available in the online journal.)

166), and 20% (34/166) of the cluster stars in this metallicity regime. Extending this break down to the entire sample gives a similar distribution of 48% (96/202), 34% (69/202), and 18% (37/202), respectively. This distribution is perhaps tied to the "primordial," "intermediate," and "extreme" populations of the O–Na anticorrelation (Carretta et al. 2008). However, only the intermediate Al subpopulation is present at all metallicities. The very enhanced Al stars ([Al/Fe] $>$ +1) are only found at [Fe/H] $\lesssim -1.2$, and the sequence of low-Al stars ([Al/Fe] $<$ +0.60) essentially terminates at about the same metallicity cutoff (this is particularly evident in the bottom panel of Figure 8). A two-sample K–S test confirms the same result as the Na case, which is that the [Al/Fe] distribution for stars with [Fe/H] >-1.2 and [Fe/H] < -1.2 are different at the 94% level.

These data suggest that ω Cen's metal-rich populations may be significantly more chemically homogeneous than the metal-poor (and presumably older) populations, but the gas from which the metal-rich stars formed was enhanced in light elements at a level beyond what is thought to be possible from Type II SNe (e.g., Woosley & Weaver 1995; Chieffi & Limongi 2004). Evidently, at high metallicity it is possible to produce Na in greater quantities than Al.

4.2. α Elements

The α elements are often used to gauge the relative contributions from Type II SNe, which are efficient producers of α elements, and Type Ia SNe, which produce mostly Fe-peak elements. Predicted stellar yields from core collapse SNe weighted by a Salpeter initial mass function (IMF; $x = 1.35$) produce [α/Fe] $\sim$ +0.30 to +0.50 across a broad range of metallicities (e.g., Chieffi & Limongi 2004). Therefore, values of [α/Fe] $\sim$ +0.10 or less suggest Type Ia SNe have contributed some portion of the Fe-peak elements. The most commonly measured α elements are O, Mg, Si, Ca, and Ti; however, Ti is more complicated because it has multiple production sources. In globular clusters, a large portion of the stars have had their O and Mg abundances altered by proton-capture nucleosynthesis and therefore these elements cannot be treated as "pure" α elements. This restricts discussions regarding α enhancement to the heavier elements.

Previous studies of ω Cen and other globular clusters have shown nearly all stars to be α enhanced at [α/Fe] $\sim$ +0.40 with very small star-to-star scatter (e.g., see review by Gratton et al. 2004). Our results are consistent with previous work and give $\langle$[Ca/Fe]$\rangle$ = +0.36 (σ = 0.09). Although Ti may straddle being classified as an α or Fe-peak element, the stars in our sample are mostly Ti-enhanced with $\langle$[Ti/Fe]$\rangle$ = +0.23 (σ = 0.14). We do not find any stars to be α-poor and our lowest derived value is [Ca/Fe] = +0.17, but a handful of α-poor stars have been found in this cluster (e.g., Norris & Da Costa 1995; Smith et al. 1995, 2000; Pancino et al. 2002). We do not find any trend in [Ca/Fe] with [Fe/H], which is in contrast to the results of Pancino et al. (2002) who find the most metal-rich stars to be α-poor. However, there is real scatter in [α/Fe] in this cluster as is evident in the Si and Ca line strength variations seen in the top panel of Figure 7. In any case, larger sample sizes are required to settle this issue, but it seems that the majority of ω Cen stars are α-rich and thus Type Ia SNe have not contributed much to the [X/Fe] ratios. This is a significant problem from a chemical evolution standpoint because either the ejecta from Type Ia SNe were preferentially lost or their presence was suppressed despite a several Gyr timespan in star formation.

4.3. Fe and Fe-Peak Elements

As mentioned above, Fe-peak elements are produced in both Type II and Type Ia SNe in copious amounts and are the most commonly used tracers of metallicity in stars. These elements are produced in similar conditions during the late stages of stellar evolution and as a result often track together as a function of overall metallicity. Aside from Fe, the other Fe-peak elements analyzed here reproduce this trend with $\langle$[Sc/Fe]$\rangle$ = +0.09 (σ = 0.15) and $\langle$[Ni/Fe]$\rangle$ = −0.04 (σ = 0.09). In both cases, there is no trend in [X/Fe] with [Fe/H]. However, since ω Cen hosts multiple stellar populations, the behavior of [Fe/H] is not as simple as most monometallic globular clusters.

Large sample spectroscopic and photometric observations of ω Cen (e.g., Norris & Da Costa 1995; Suntzeff & Kraft 1996; van Leeuwen et al. 2000; Rey et al. 2004; Sollima et al. 2005a; Villanova et al. 2007; Johnson et al. 2008) have shown that the cluster hosts multiple populations of stars with almost no stars being more metal-poor than [Fe/H] = −2, more than half having [Fe/H] $\approx$ −1.7, and the rest forming a high-metallicity tail extending to [Fe/H] $\sim$ −0.5. Again combining our new results with those from Johnson et al. (2008), we have a homogeneous set of spectroscopically determined [Fe/H] abundances for 228 RGB stars. In Figure 9, we show a histogram of our combined sample and our results are consistent with the cluster having multiple peaks in the metallicity distribution function at [Fe/H] = −1.75, −1.45, −1.05, and −0.75. These peaks constitute roughly 55%, 30%, 10%, and 5% of our observations, respectively. The percentage of stars contained in each population is nearly identical between our entire sample and a subset having the highest completion fraction ($V \leqslant 12.5$). This leads us to believe our full sample is representative of the entire cluster population.

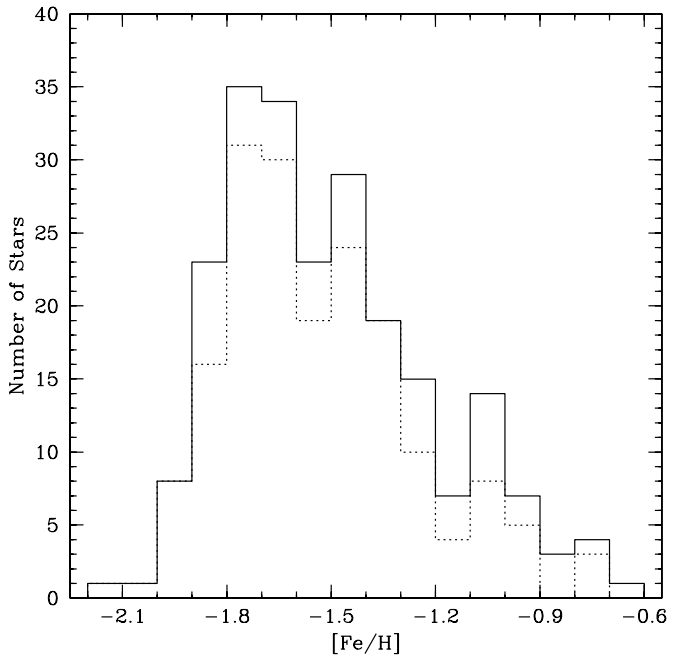

Figure 9. Histogram of derived [Fe/H] values for the combined sample of this study and Johnson et al. (2008) with bin sizes of 0.10 dex. The dashed line histogram shows the results from Johnson et al. (2008).

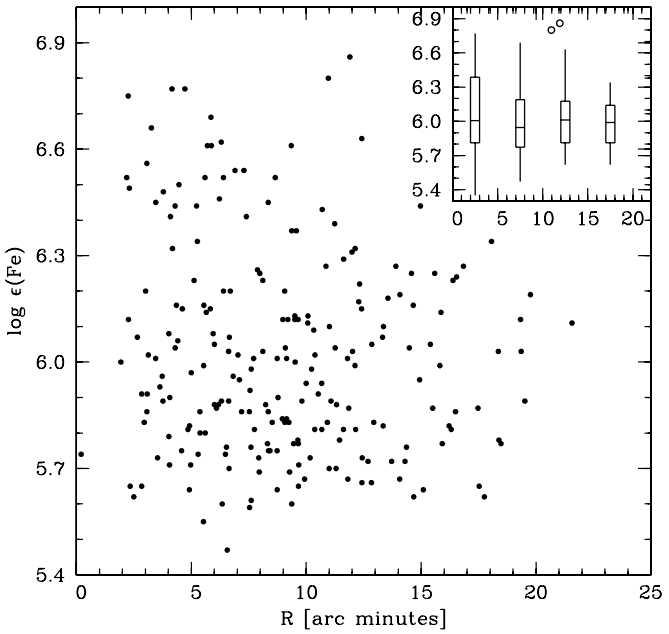

Figure 10. Fe is plotted as a function of distance from the cluster center. The points show the data from both this study and Johnson et al. (2008). We have averaged the Fe abundances for stars observed in both studies. The inset plot shows the mean and quartile distributions in 5′ bins. The vertical lines represent the full data range (except outliers) and the open circles indicate mild outliers between 1.5 and 3.0 times the interquartile range.

In addition to ω Cen being chemically diverse, there is some evidence for a cluster metallicity gradient such that the inner regions contain most of the metal-rich stars (e.g., Suntzeff & Kraft 1996; Norris et al. 1996 Hilker & Richtler 2000; Pancino et al. 2003; Johnson et al. 2008). These results are confirmed in photometric studies (e.g., Rey et al. 2004), which show that the anomalous, metal-rich RGB (RGB-a) is found only near the core of the cluster. In Figure 10, we plot log ϵ(Fe) versus distance from the cluster center. We find that the most metal-rich stars are mostly located inside 10′, but the metal-poor stars are located uniformly throughout the cluster. The inset plot in Figure 10 shows that the median metallicity stays constant at about log ϵ(Fe) = 6.0 ([Fe/H] ≈ −1.5) at all radii, but the metallicity interquartile and full ranges decrease at large radii. There has been speculation that, in addition to these spatial anomalies, the various cluster populations may exhibit unique kinematic signatures as the result of the cluster formation process (e.g., Norris et al. 1997; Sollima et al. 2005b). However, recent larger sample studies seem to indicate that none of ω Cen's subpopulations exhibit rotational, proper motion, or radial velocity anomalies (Reijns et al. 2006; Pancino et al. 2007; Johnson et al. 2008; Bellini et al. 2009). These new results seem to negate the merger and background cluster superposition scenarios.

4.4. Neutron-Capture Elements

Most elements heavier than the Fe-peak are produced via successive neutron captures on seed nuclei, but a limited number of these elements have optical atomic transitions. In the metallicity regime considered here, Ba and La are often the primary tracers of the main *s*-process component and Eu the primary tracer of the *r*-process. As previously mentioned, nearly all globular clusters are *r*-process-rich with [Eu/Ba, La] ≈ +0.25 (e.g., Gratton et al. 2004), but previous studies have shown that ω Cen has very strong *s*-process enhancement, especially at [Fe/H] $\gtrsim$ −1.5 (e.g., Francois et al. 1988; Norris & Da Costa 1995; Smith et al. 1995, 2000). We find in agreement with previous studies that most ω Cen stars more metal-rich than [Fe/H] ∼ −1.7 are strongly *s*-process enriched based on [La/Eu] ratios approaching and exceeding +0.8. While the most metal-poor stars have ⟨[La/Eu]⟩ = −0.02, this value rises to ⟨[La/Eu]⟩ = +0.49 by [Fe/H] ∼ −1.4 meaning that [La/Eu] increases by more than a factor of 3 during a span in which [Fe/H] increases by a factor of 2. However, we find that ⟨[La/Fe]⟩ does not increase appreciably at metallicities exceeding [Fe/H] ∼ −1.2 (excluding possible Ba-stars), but all stars in our sample with [Fe/H] > −1.2 have [La/Fe] > +0.5 and abundance patterns dominated by the *s*-process. This trend is not shared by Eu, which remains mostly constant at ⟨[Eu/Fe]⟩ = +0.19 (σ = 0.23) at all metallicities. We have also found that 25% (15/60) of our sample may qualify as Ba-stars with [La/Fe] ⩾ +1.0. The most extreme case is star LEID 45358, which has [La/Fe] = +2.03 and [La/Eu] = +1.81. For stars in common between the two samples, van Loon et al. (2007) found these to have large Ba4554 indices indicating they are Ba-rich as well.

5. DISCUSSION

5.1. Chemical Enrichment in ω Cen

Spectroscopic and photometric analyses of ω Cen stars have revealed a system hosting a complex past. The cluster metallicity apparently increased from [Fe/H] ≈ −2.2 to [Fe/H] ≈ −0.5 over roughly 2–4 Gyr (e.g., Stanford et al. 2006) and ω Cen has experienced a handful of discrete star formation events. The metallicity distribution peaks in our data agree with those found in the literature and correspond to the "MP" ([Fe/H] ∼ −1.7), "MINT2" ([Fe/H] ∼ −1.4), "MINT3" ([Fe/H] ∼ −1.0), and "SGB-a" ([Fe/H] ∼ −0.6) populations found on the SGB by Sollima et al. (2005b). However, these classifications are not as well defined on the main sequence and show considerable complexity (e.g., Bedin et al. 2004; Piotto et al. 2005; Villanova

et al. 2007). The apparent kinematic homogeneity of the various stellar populations (e.g., Pancino et al. 2007; Bellini et al. 2009) suggests most, if not all, of the cluster's chemical enrichment is the result of internal processes rather than a product of multiple merger events. However, the paucity of stars more metal-poor than [Fe/H] ~ -2 means the nascent gas from which the primary population formed was already considerably polluted by massive star ejecta. One of the most striking results discovered so far is that the second most metal-poor stellar population ([Fe/H] ~ -1.4; and perhaps the subsequent more metal-rich stars) may have experienced both a huge increase in He content (dY/dZ $\sim$ 70; Piotto et al. 2005) and an equally impressive increase in *s*-process element abundances compared to the primary population ([Fe/H] ~ -1.7), which contains more than half of all ω Cen stars. Somehow these events took place while preserving the various light element correlations observed in other globular clusters that do not (in general) have large He and metallicity variations and lack strong *s*-process signatures. Since the combined Johnson et al. (2008) and current data sets allow us to probe various production sources, we turn now to what our current data add to ω Cen's puzzling past.

5.1.1. Supernova Pollution

The majority of elements heavier than Li are produced during various quiescent and explosive nucleosynthetic events in $\gtrsim$11 $M_\odot$ stars (Woosley & Weaver 1995). These processes, which occur within $\lesssim 20 \times 10^6$ yr after the onset of star formation, are known to produce an overabundance of α elements by about a factor of 2 relative to the solar α/Fe ratio. In addition, massive stars also produce varying amounts of the odd-Z light elements (e.g., C through Al) with metallicity dependent yields of $-0.5 \lesssim$ [X/Fe] $\lesssim +0.3$ in the metallicity regime covered by ω Cen stars (e.g., Woosley & Weaver 1995; Chieffi & Limongi 2004; Nomoto et al. 2006). Although the final abundances of Fe-peak elements are dependent on the explosion energy and mass cut, they generally track closely to Fe. These stars inevitably produce some neutron-capture elements as well, but only the lower mass SNe ($\sim$8–11 $M_\odot$) are believed to be significant *r*-process contributors (e.g., Mathews & Cowan 1990; Cowan et al. 1991; Wheeler et al. 1998), while low-mass AGB stars ($\sim$1–4 $M_\odot$) seem to be the best candidates for *s*-process production (e.g., Busso et al. 1999).

In contrast, mass transfer Type Ia SNe may take anywhere from 500×10^6 to more than 3×10^9 yr to evolve (e.g., Yoshii et al. 1996) and could have difficulty forming in low-metallicity ([Fe/H] < -1) environments (Kobayashi et al. 1998). Nucleosynthesis calculations have shown that these SNe predominantly produce Fe-peak elements and only trace amounts of α and light elements (Nomoto et al. 1997). It is estimated that Type Ia SNe have produced at least 50% of the total ^{56}Fe in the Galaxy and their onset is believed to be the primary cause for the decline in [α/Fe] at [Fe/H] > -1 in the disk and halo populations. It is for this reason that the [α/Fe] ratio is often used as a diagnostic to test the presence of Type Ia SNe in a stellar system.

While there have been some α-poor stars found in ω Cen's most metal-rich population (Pancino et al. 2002), the general trend of enhancement in the α elements suggests that a majority of the cluster's chemical evolution occurred before Type Ia SNe had time to evolve. Determining whether or not Type Ia SNe can form in metal-poor environments could help place additional constraints on ω Cen's evolutionary timescale. If the lower limit of [Fe/H] ~ -1 estimated by Kobayashi et al. (1998) is correct and only the most metal-rich population in the cluster is affected by Type Ia SNe ejecta, then this would imply an age difference between the [Fe/H] ~ -1 and [Fe/H] ~ -0.7 groups of $\lesssim$1 Gyr. However, if this limit is at a much lower metallicity, then the cluster would have had to evolve on a much shorter timescale.

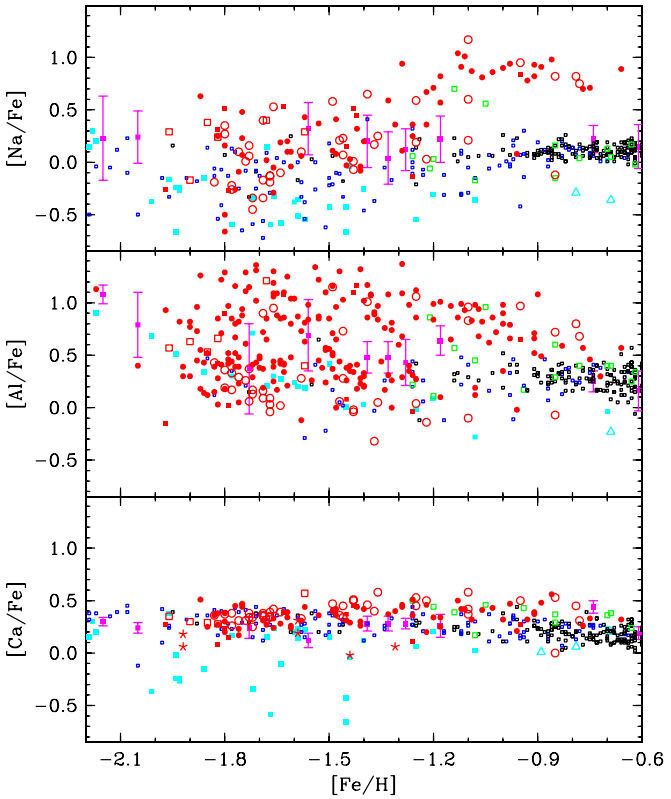

Figure 11. Plots of [Na/Fe], [Al/Fe], and [Ca/Fe] vs. [Fe/H] are shown with data from this study and the literature. The filled circles are values from the combined sample of this study and Johnson et al. (2008), the open circles are from Norris & Da Costa (1995), the filled squares are from Smith et al. (2000), the open squares are from Francois et al. (1988), and the stars are from Smith et al. (1995). Literature values are provided for the thin/thick disk (open black boxes), halo (open blue boxes), bulge (open green boxes), dwarf spheroidals (filled cyan boxes), globular clusters with 1σ bars (filled magenta boxes), and the Sagittarius dwarf spheroidal (open cyan triangles). References are given in Table 5.

(A color version of this figure is available in the online journal.)

In Figures 11–13, we show the evolution of all elements measured in this study as a function of [Fe/H] along with those available in the literature for ω Cen, the Galactic disk, bulge, halo, globular clusters, and nearby dwarf spheroidal galaxies (see Table 5 for data references). From these data we have confirmed: (1) a more than 1.0 dex spread exists for [Na/Fe] and [Al/Fe] and the two elements are correlated; (2) the α elements are enhanced by about a factor of 2 at all metallicities with small star-to-star scatter; (3) there are at least four different metallicity peaks (see also Figure 9) at [Fe/H] $= -1.75, -1.45, -1.05, -0.75$ with internal dispersions of $\sim$0.10 dex in each subpopulation; and (4) there is a large *s*-process component that manifests itself in the intermediate and metal-rich populations of the cluster. As is the case for other globular clusters, the larger star-to-star variations seen in the light and neutron-capture elements versus the α and Fe-peak elements suggest additional production (or destruction) sources other than core-collapse SNe. We know that, at least for the light elements, the observed inhomogeneity is not due to incomplete mixing of SN ejecta

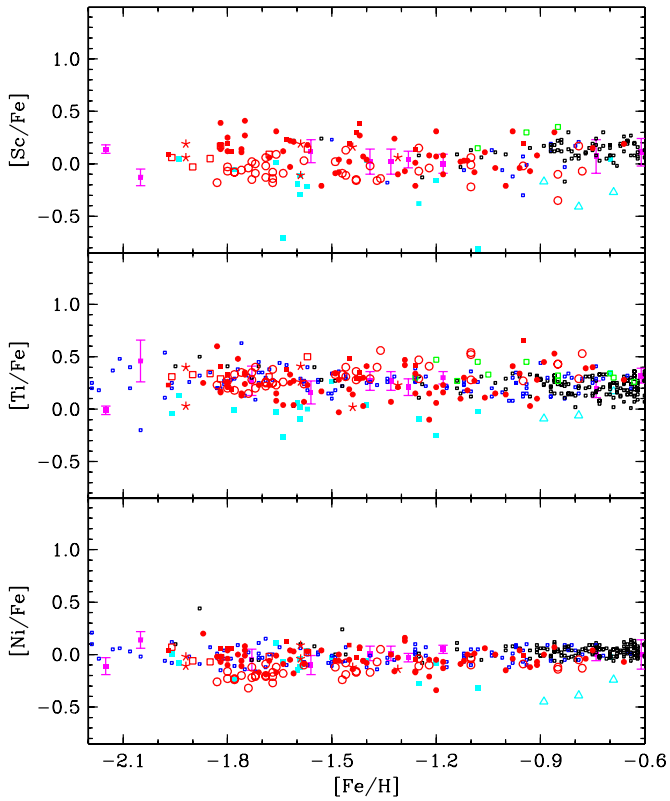

Figure 12. Plots of [Sc/Fe], [Ti/Fe], and [Ni/Fe] vs. [Fe/H] are shown with data from this study and the literature. The symbols and [X/Fe] scales are the same as in Figure 11.

(A color version of this figure is available in the online journal.)

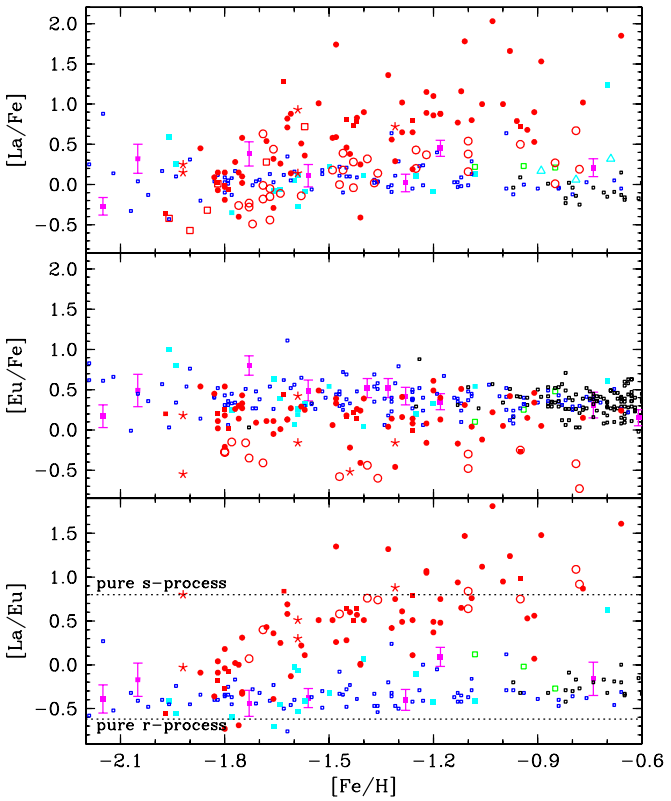

Figure 13. Plots of [La/Fe], [Eu/Fe], and [La/Eu] vs. [Fe/H] are shown with data from this study and the literature. The symbols are the same as in Figure 11. The dashed lines indicating pure *s*-process and *r*-process abundance ratios are taken from McWilliam (1997).

(A color version of this figure is available in the online journal.)

because the Na/Al enhanced stars are also O-poor (e.g., Norris & Da Costa 1995; Smith et al. 2000).

If massive stars cannot account for all of the observed abundance anomalies in ω Cen, then how much can they account for? At least in stars with [Fe/H] < -1, Type II SNe are responsible for producing nearly all of the α and Fe-peak elements. However, IMF weighted theoretical yields of SNe with initial metallicities in the range $-2 <$ [Fe/H] < -0.5 (e.g., Woosley & Weaver 1995; Chieffi & Limongi 2004; Nomoto et al. 2006) produce values roughly consistent with those observed in the disk, halo, and bulge (i.e., ⟨[Na/Fe]⟩ ∼ 0; ⟨[Al/Fe]⟩ ∼ +0.3), but ω Cen (and other globular cluster) stars can reach [Na/Fe] ∼ +1.0 and [Al/Fe] ∼ +1.4. Using the Al data in Figure 11 to trace the percentage of stars with light element abundance patterns matching those observed in the other Galactic populations at comparable metallicity ([Al/Fe] $\leqslant$ +0.5), we find 42% (84/202) of our sample fall into this category. It is more difficult to quantify this with the Na data because the sample size is more than a factor of 3 smaller, but it appears that at least a significant fraction of the stars in Figure 11 with [Fe/H] < -1.2 show [Na/Fe] ratios consistent with the disk, halo, and bulge, but nearly all of the more metal-rich stars are enhanced in Na. This further solidifies the claim that although Type II SNe have had a significant impact on all ω Cen stars, they are not the only significant nucleosynthesis site. Assuming our data are representative, roughly half of all ω Cen stars appear to have formed in an environment that was polluted with the ejecta from sources other than Type II SNe.

Further inspection of Figure 11 reveals an interesting trend in Na and Al as a function of [Fe/H]. As noted in Section 4.2, there is a clear lack of stars showing Na and Al abundances consistent with being polluted solely by Type II SNe at [Fe/H] $\gtrsim -1.2$. Only 6% (1/17) of ω Cen giants are "Na-normal" ([Na/Fe] ∼ 0), and this trend is present in both the Norris & Da Costa (1995) and Smith et al. (2000) data as well. A similar result is observed in the larger sample of Al data in that only 22% (8/36) are "Al-normal" ([Al/Fe] $\lesssim$ +0.3). While there appears to be a downturn in the maximum [Al/Fe] attained at [Fe/H] > -1.2, the rise in [Na/Fe] and [La/Fe] coupled with the stability of [α/Fe] and [Eu/Fe] in the same metallicity range indicates this artifact is not the result of Type Ia SNe adding Fe but instead a decrease in the [Al/Fe] ratio being added to the cluster's interstellar medium (ISM) by the production source. What is perhaps most intriguing is that despite a (possible) huge increase in He between the [Fe/H] $= -1.7$ and –1.4 groups, the light element trends are very similar. It would seem that whichever stars are the source of the high He abundances do not produce abnormally large [Na/Fe] and [Al/Fe] ratios because similar enhancements in Na and Al are found in globular clusters that do not show signs of such extreme He variations.

If Eu production can be attributed mostly to 8–10 $M_{\odot}$ stars, then we know from those data alone that chemical enrichment had to have occurred in ω Cen over more than $\sim 200 \times 10^6$ yr because there are at least four subpopulations with different [Fe/H] and [Eu/Fe] is roughly constant (with some scatter). However, [Eu/Fe] is, on average, consistently at least 0.1–0.2 dex underabundant relative to the other populations shown in Figure 13. The reason for this is not clear, but it could be that the ratio of 8–10 $M_{\odot}$ versus higher mass stars was anomalously low in ω Cen relative to other systems.

Table 5
Literature References for Figures 11–16

Object	Reference
Thin/thick disk	Bensby et al. (2003)
Thin/thick disk	Bensby et al. (2005)
Thin/thick disk	Fulbright (2000)
Thin/thick disk	Fulbright et al. (2007)
Thin/thick disk	Reddy et al. (2003)
Thin/thick disk	Simmerer et al. (2004)
Halo	Fulbright et al. (2000)
Halo	Reddy et al. (2006)
Halo	Simmerer et al. (2004)
Bulge	McWilliam & Rich (1994)
Bulge	Fulbright et al. (2007)
Bulge	Lecureur et al. (2007)
Dwarf spheroidals	Shetrone et al. (2001)
Dwarf spheroidals	Shetrone et al. (2003)
Sagittarius dwarf	Sbordone et al. (2007)
Globular cluster (M4)	Ivans et al. (1999)
Globular cluster (M5)	Ivans et al. (2001)
Globular cluster (M13)	Sneden et al. (2004)
Globular cluster (M13)	Johnson et al. (2005)
Globular cluster (M15[a])	Sneden et al. (1997)
Globular cluster (M68[a])	Lee et al. (2005)
Globular cluster (M71)	Ramírez & Cohen (2002)
Globular cluster (M80)	Cavallo et al. (2004)
Globular cluster (47 Tuc)	Carretta et al. (2004)
Globular cluster (47 Tuc)	James et al. (2004)
Globular cluster (NGC 288)	Shetrone & Keane (2000)
Globular cluster (NGC 362)	Shetrone & Keane (2000)

Note. [a] These two clusters have had their measured [Fe/H] values shifted by +0.2 dex to fit in Figures 11–14. These shifts were not applied to the displayed [X/Fe] abundances.

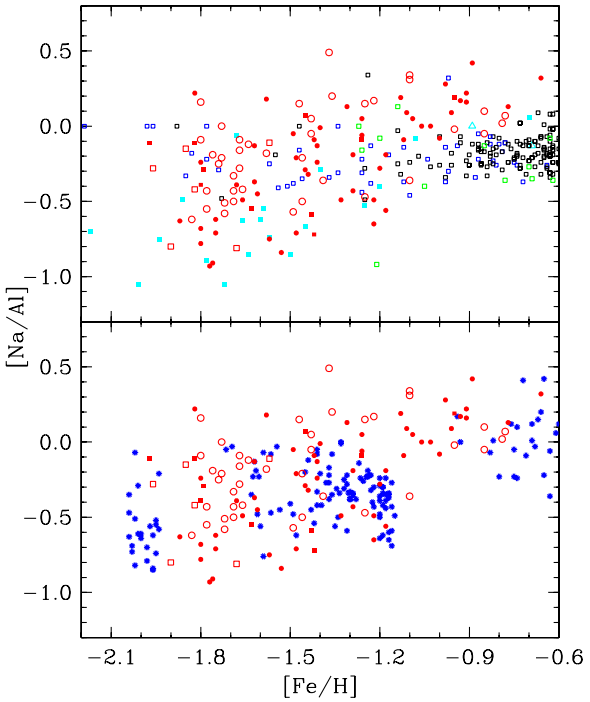

Figure 14. [Na/Al] ratios as a function of metallicity are shown for a variety of populations. The symbols in the top panel are the same as those in Figure 11 and the blue points in the bottom panel represent individual globular cluster stars.
(A color version of this figure is available in the online journal.)

5.1.2. Intermediate-Mass AGB Stars

The discovery of significant star-to-star scatter in light elements coupled with the O–Na anticorrelation in stars on the main sequence and subgiant branches of globular clusters seems to indicate that the various relations among the elements O through Al were already imprinted on the gas from which the current generations of stars formed. As discussed in Section 1, HBB occurring in intermediate-mass ($\sim$5–8 $M_{\odot}$) AGB stars is currently favored as a likely location for producing the light element trends. These stars have the advantages of preserving their initial [Fe/H] envelope abundances, ejecting enriched material at low velocities, experiencing few third dredge-up episodes (negligible *s*-process production), and reaching envelope temperatures $>70 \times 10^6$ K that activate the NeNa and MgAl proton-capture cycles. However, current AGB stellar models are highly sensitive to the adopted treatment of convection and mass loss and it has been pointed out that these scenarios do not explain the role of super-AGB stars (those that ignite core carbon but not neon burning) nor 1–4 $M_{\odot}$ AGB stars (Prantzos & Charbonnel 2006). Models using standard mixing length theory (e.g., Fenner et al. 2004; Karakas & Lattanzio 2007) are unable to reproduce the large O depletions ([O/Fe] < -0.6) found in some globular cluster stars (including ω Cen) and show large enhancements in [C + N + O/Fe], which conflict with observations that the CNO sum is constant (Pilachowski 1988; Dickens et al. 1991; Norris & Da Costa 1995; Smith et al. 1996; Ivans et al. 1999). On the other hand, models adopting the full spectrum of turbulence treatment of convection (e.g., Ventura & D'Antona 2008) show fewer third dredge-up episodes and thus keep the CNO sum roughly constant while explaining some of the C through Al abundance trends seen in globular clusters. Neither case is able to fully explain all light element anomalies, in particular the super O-poor stars and Mg isotopic ratios, which may require a hybrid scenario that includes in situ deep mixing and HBB in $\gtrsim$5 $M_{\odot}$ AGB stars (e.g., D'Antona & Ventura 2007) in addition to improvements in key nuclear reaction rates.

Can these stars reproduce what we observe in ω Cen? Our data have shown that only about half of the stars in our sample are consistent with being formed from gas predominantly polluted by Type II SNe (i.e., the stars are not particularly enhanced in Na and Al compared to disk and halo stars of comparable metallicity). Since $>5\,M_{\odot}$ AGB stars likely do not alter the abundances of any elements heavier than Al, we will restrict the discussion to those elements. First turning to the populations with [Fe/H] < -1.2, the stars with [Na/Fe] > 0 and [Al/Fe] $> +0.5$ have envelope material that was likely exposed to high-temperature proton-capture processing in an external environment. Although the light element yields are sensitive to both model parameters and nuclear reaction rates, the Ventura & D'Antona (2008) results indicate that intermediate-metallicity 5–6.5 $M_{\odot}$ AGB stars can produce $+0.30 <$ [Na/Fe] $< +0.60$ and [Al/Fe] $\sim +1.0$, while the Fenner et al. (2004) data predict somewhat higher Na and lower Al abundances. These values are consistent with the "intermediate" Al population that has $\langle$[Al/Fe]$\rangle = +0.82$ ($\sigma = 0.10$) and suggest intermediate-mass AGB stars could be responsible for the enhancements seen in these stars. However, about 20% of the stars with [Fe/H] < -1.2 have [Al/Fe] $> +1$ and [Na/Fe] $> +0.5$. These stars are not accounted for by current AGB models and may have undergone additional in situ deep mixing or require pollution from another unknown source.

As can be seen in the top panel of Figure 14, halo, disk, and bulge stars exhibit a roughly constant [Na/Al] ≈ -0.2

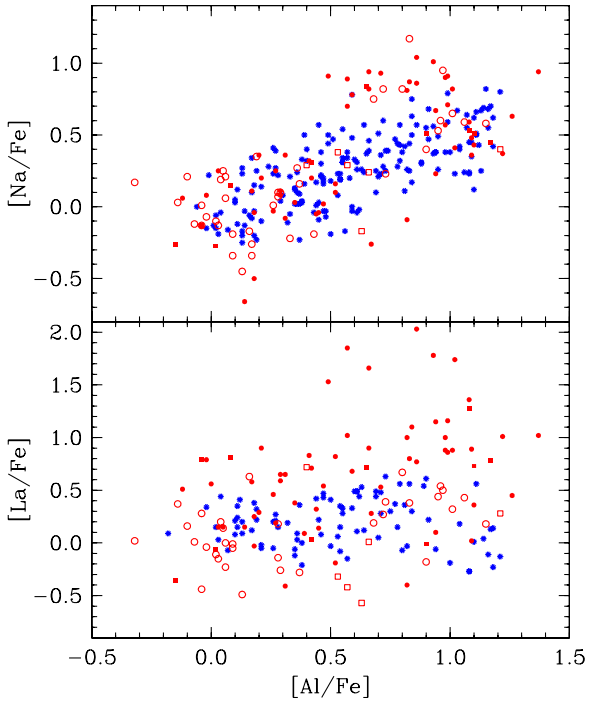

Figure 15. Top panel shows [Na/Fe] vs. [Al/Fe] and compares ω Cen data to results from individual globular cluster stars. The bottom panel shows the same set of stars but plots [La/Fe] vs. [Al/Fe]. The symbols are the same as those in Figure 14.

(A color version of this figure is available in the online journal.)

from [Fe/H] = −2 to −0.6, while ω Cen, dwarf spheroidal, and globular cluster stars display a wide range from [Na/Al] = −1 to +0.4 and show a general increase in ⟨[Na/Al]⟩ with increasing metallicity. Since the final abundances of Na and Al in SN ejecta scale similarly with neutron excess and metallicity (Arnett 1971), the Na/Al ratio is mostly insensitive to metallicity changes and is consistently near [Na/Al] ∼ −0.2 (e.g., Woosley & Weaver 1995). The overproduction of Al at low metallicities and underproduction at higher metallicities is consistent with the observed trends in AGB models (e.g., Ventura & D'Antona 2008) due to lower temperatures at the bottom of the convective envelope and shallower mixing in more metal-rich stars. This trend is nearly identically reproduced in globular cluster stars of varying metallicity (bottom panel of Figure 14) and likely indicates the same stars that are responsible for the globular cluster light element anomalies are also prevalent in ω Cen. Since the same trend is also observed in dwarf spheroidal stars, which are not believed to be strongly enriched in Type II SN ejecta, this may strengthen the case for HBB in intermediate-mass AGB stars (or some equivalent H-burning environment) to be the source of light element abundance trends different than those seen in the disk and halo. It is interesting that these two systems share the rise in [Na/Al] versus [Fe/H] with globular clusters because, as their low [α/Fe] ratios indicate, star formation has proceeded much differently in dwarf spheroidals despite having comparable main-sequence turnoff age ranges with ω Cen.

The paucity of stars with [Al/Fe] > +1 at [Fe/H] > −1.2 is also consistent with the predictions of in situ deep mixing at higher metallicities where the increased μ-gradient is expected to inhibit dredge-up of ON, NeNa, and MgAl cycled material into the stellar envelope via meridional circulation (e.g., Sweigart & Mengel 1979). While the range in Na and Al data track closely to that of other globular clusters at low and intermediate metallicity, the more metal-rich ω Cen stars show surprising Na enhancements and decreased star-to-star scatter that are not seen in globular clusters of comparable metallicity. This is true even for M4 ([Fe/H] ∼ −1.1), which is suspected of having a second, more enriched population without a large spread in Fe (Marino et al. 2008). Although the range of M4's Al abundances are consistent with the values we find here, the *average* [Na/Fe] ratio in ω Cen giants of comparable metallicity is about 0.3 dex larger than the highest [Na/Fe] abundance found by either Ivans et al. (1999) or Marino et al. (2008) in M4. It would seem that there was an additional source of Na in the more metal-rich ω Cen populations or that hardly any unenriched gas remained to dilute the AGB ejecta. Figure 15 illustrates this point in that the stars with [Fe/H] > −1.2 and [Al/Fe] > +0.5 have [Na/Fe] ratios that lie above the range expected for a given Al abundance based on typical globular cluster values. The identity of the Na source is only speculative, but if the progenitor AGB population that polluted the gas from which the [Fe/H] > −1.2 stars formed was He-rich, the higher temperatures and possible deeper mixing in regions where the NeNa cycle was operating may have contributed to the increased Na abundances. It may also be possible that lower mass, He-rich AGB stars, which evolve more quickly than He-normal stars (and produce more Na and less Al), could have a larger impact than in normal globular clusters. However, $\lesssim$4 $M_{\odot}$ AGB stars are not believed to strongly deplete O and would have to already be O-poor to reproduce the subsolar [O/Fe] ratios found in many ω Cen giants with [Fe/H] $\gtrsim$ −1.5.

5.1.3. Low-Mass AGB Stars

Lower mass, thermally pulsing AGB stars (∼1–4 $M_{\odot}$), which evolve over 150 × 10^6–2.5 × 10^9 yr (Schaller et al. 1992), are thought to be the primary producers of the main *s*-process component in the Galaxy at metallicities found in ω Cen (e.g., Busso et al. 2001). Smith et al. (2000) showed that the [Rb/Zr] ratio in ω Cen was consistent with the *s*-process being produced in 1.5–3.0 $M_{\odot}$ AGB stars, implying a monotonic, total evolutionary timescale of ∼2–3 Gyr. This is consistent with most other estimates (e.g., Stanford et al. 2006; but see also Villanova et al. 2007). Since these stars have the longest formation timescale, the presence of their chemical signatures sets a lower limit on relative age estimates.

The halo and disk populations are known to exhibit a steady rise in the contribution of *s*-process elements at [Fe/H] > −2.5 (e.g., Simmerer et al. 2004), but globular cluster heavy element abundances are dominated by the *r*-process (e.g., Gratton et al. 2004) and are indicative of the rather rapid chemical evolution timescales of normal globular clusters compared to the disk and halo. Interestingly, dwarf spheroidal stars tend to have a stronger *s*-process component than any of the Galactic populations (e.g., Geisler et al. 2007), but one that is much smaller than that seen in ω Cen. This, along with the evidence for Type Ia SN pollution, implies dwarf spheroidal galaxies evolve much differently than most other Galactic stellar systems and do so with a rather subdued star formation rate (e.g., Mateo 2008).

However, the Galactic bulge is believed to have formed rapidly, as constrained by turnoff photometry (Ortolani et al. 1995; Kuijken & Rich 2002; Zoccali et al. 2003; Clarkson et al. 2008) as well as by measured high [α/Fe] (e.g., McWilliam & Rich 1994; Fulbright et al. 2006; Lecureur et al. 2007). Theoretical studies argue for timescales significantly less than 10^9 yr (e.g., Elmegreen 1999; Elmegreen et al. 2008; Ballero

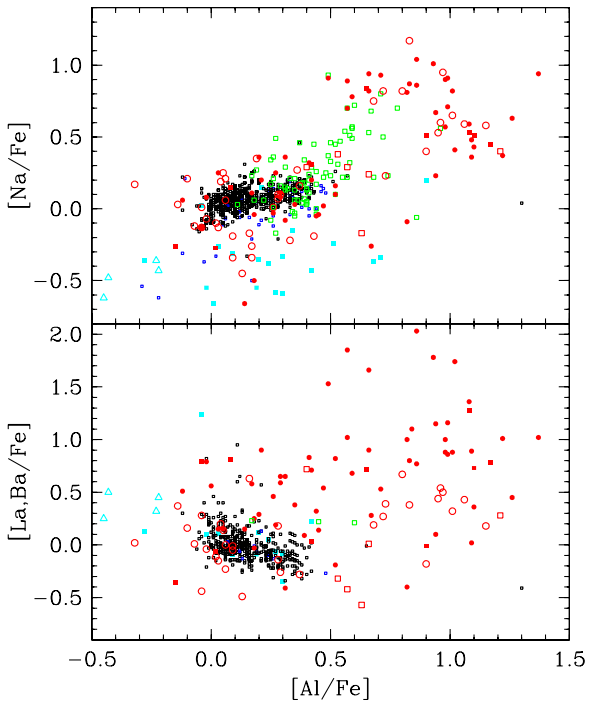

Figure 16. Top panel shows [Na/Fe] vs. [Al/Fe] with data from this study and the literature. The bottom panel shows [La,Ba/Fe] vs. [Al/Fe] where the Ba data are used as a tracer for the *s*-process in the disk and halo while La is used in all other cases. The symbols are the same as those in Figure 11.

(A color version of this figure is available in the online journal.)

et al. 2007). Yet despite a metallicity that is high compared to the halo and ω Cen (e.g., Fulbright et al. 2006; Zoccali et al. 2008), the *s*-process elements are seen to exhibit solar [X/Fe] ratios (McWilliam & Rich 1994) that would appear to require low- and intermediate-mass stars to have provided significant input to the bulge's chemical evolution.

In Figure 13, we show the evolution of [La/Fe], [Eu/Fe], and [La/Eu] as a function of [Fe/H] for ω Cen and other stellar populations. Since all but the most metal-poor group of ω Cen stars show significant enhancement in the *s*-process element La (and the [La/Eu] ratio), we find in agreement with previous studies that at least 10^9 yr had to have passed between the formation of the primary population at [Fe/H] $= -1.7$ and the final population at [Fe/H] $= -0.7$ to allow the low-mass progenitor populations enough time to evolve. A significant percentage (25%) of stars in our sample have [La/Fe] $\geqslant +1.0$ and may be the result of binary mass transfer from a $< 4\ M_{\odot}$ AGB companion. However, none of these stars are present in the dominant, most metal-poor population but are found at [Fe/H] > -1.5 with most being present at [Fe/H] > -1. It is unknown whether the prevalence of such stars at higher metallicities is a result of the longer formation timescales needed for one of the companions to evolve, an anomalous increase in the binary fraction at higher metallicity, or a sample selection effect. If the result is not a selection effect, then this may be a clear indication that the more metal-rich stars are at least (1–2) $\times\ 10^9$ yr older than the metal-poor population.

Figures 15 and 16 show [Na/Fe] and [La/Fe] versus [Al/Fe], which could be a useful indicator regarding the relative importance of low- versus intermediate-mass AGB stars. In most globular clusters, there is little evidence of light elements showing any correlation with heavy neutron-capture elements on top of the correlations seen among the various light elements (e.g., Smith 2008), which implies the elements lighter than Al are produced in a different astrophysical site over different timescales than those produced via the *s*-process and *r*-process. This may mean that the current generation of globular cluster stars have abundance signatures strongly weighted toward pollution from more massive AGB stars compared to those $\lesssim 4\ M_{\odot}$. On the contrary, ω Cen exhibits a mild correlation between La and Al (as well as Na) and as stated above shows [La/Fe] ratios well in excess of the roughly [La/Fe] $\sim +0.5$ maximum found in globular cluster stars, especially at [Fe/H] > -1.5. Current AGB nucleosynthesis models (e.g., Ventura & D'Antona 2008) suggest that this correlation is unlikely to be the result of $\sim$1–4 $M_{\odot}$ stars dominating the chemical enrichment of ω Cen because AGB stars in that mass range are shown to produce Na without significantly depleting O, which contradicts the O–Na anticorrelation observed in the cluster giants and prevalence of O-poor stars at higher metallicities (e.g., Norris & Da Costa 1995). For the other populations shown in Figure 16, only the bulge data show any hint of a Na–Al correlation, but that is not believed to be the result of the same mechanism at work in globular clusters (Lecureur et al. 2007). However, the current lack of heavy element data in the bulge makes it difficult to draw conclusions regarding the impact of low-mass AGB stars in that environment. Since none of the other populations show any correlation between La and Al (or Na), it appears that ω Cen is (as always) a special case where both low- and intermediate-mass AGB stars have had significant influence on the cluster's chemical evolution.

In this paper and previous studies, it has been shown that ω Cen is an extremely complex object with an intriguing formation history. Nearly all aspects of its past remain a mystery and although it has been shown that the cluster experienced multiple star formation episodes (and probably significant mass loss), there is evidence both for and against simple monotonic chemical enrichment (i.e., metal-poor stars are older than more metal-rich stars). It appears that ω Cen shares many chemical characteristics with a variety of systems that formed under widely different conditions and the cluster exhibits signs of both rapid and extended star formation. One of the interesting issues raised by our data is the significance of the apparent transition in light element abundance trends at [Fe/H] ≈ -1.2. It seems as if the stars with [Fe/H] > -1.2 were made almost entirely out of AGB ejecta, but the populations with [Fe/H] < -1.2 contain groups of stars that likely formed both with and without the presence of AGB pollution in nearly equal proportions. The lack of α-poor stars in all but perhaps the most metal-rich population poses a serious problem and ω Cen's enrichment history challenges the paradigm of chemical evolution that for timescales >1 Gyr, Type Ia SNe contribute Fe-peak and α-poor material that drive down the [α/Fe] ratio to near solar composition. It may be that the cluster lost too much mass before the onset of Type Ia SNe or the ejecta were located too far outside the core to be retained. This may be corroborated by evidence that there is no radial preference in the location of X-ray binaries in ω Cen due to a lack of mass segregation (e.g., Gendre et al. 2003). While the observation of large numbers of RGB, SGB, and main-sequence stars are needed to understand the full picture of ω Cen's evolution, the large fluctuations in light element abundances such as Na and Mg, which are often used as metallicity tracers, make low-resolution or integrated light studies difficult to decipher. However, future large sample, high-resolution studies spanning both the giant branches and main sequences should help further

isolate the chemical signatures of each subpopulation and allow more quantitative analyses.

6. SUMMARY

We have determined abundances of several light, α, Fe-peak, and neutron-capture elements for 66 RGB stars in the globular cluster ω Cen using moderate resolution ($R \approx 18{,}000$) spectra. Two different Hydra spectrograph setups were employed spanning 6000–6250 Å and 6530–6800 Å, yielding co-added S/N ratios of about 50–200. The observations covered the full cluster metallicity regime with an emphasis on the intermediate and metal-rich populations. The elemental abundances were determined using either equivalent width analyses or spectrum synthesis, with the addition of hyperfine structure data when available.

The light elements Na and Al show large abundance inhomogeneities that span more than a factor of 10 and the elements are correlated. The Al data set was supplemented with that from Johnson et al. (2008) and yielded [Fe/H] and [Al/Fe] abundances for more than 200 RGB stars. From these data we find evidence for the existence of possibly three different populations of stars with distinct [Al/Fe] patterns. The three sequences segment into those with $\langle$[Al/Fe]$\rangle$ = +0.34 (σ = 0.14), $\langle$[Al/Fe]$\rangle$ = +0.82 (σ = 0.10), and $\langle$[Al/Fe]$\rangle$ = +1.17 (σ = 0.11) and represent 48%, 34%, and 18% of our sample, respectively. These may be inherently tied to the "primordial," "intermediate," and "extreme" populations found in normal globular clusters that exhibit varying degrees of O depletion and Na enhancement. However, there appears to be a break in the distribution of both Na and Al at [Fe/H] ≈ -1.2. Stars with [Fe/H] < -1.2 have abundances in the range $-0.1 \lesssim$ [Al/Fe] $\lesssim +1.4$ and $-0.5 \lesssim$ [Na/Fe] $\lesssim +0.6$ with at least half of the stars exhibiting light element abundances consistent with the disk and halo populations, but more than 75% of the stars with [Fe/H] > -1.2 are enhanced in Na and Al with values exceeding those found in the disk, halo, and even some globular clusters. None of the stars with [Al/Fe] > +1.0 are found at [Fe/H] > -1.2. A two-sided K–S test reveals the Na and Al abundances on either side of the [Fe/H] $= -1.2$ cutoff to have a >90% probability of being drawn from different parent populations.

All of our program stars are enhanced in α elements with $\langle$[Ca/Fe]$\rangle$ = +0.36 (σ = 0.09) and $\langle$[Ti/Fe]$\rangle$ = +0.23 (σ = 0.14), despite showing a range of more than a factor of 30 in [Fe/H]. The Fe-peak elements share the same small range in star-to-star scatter but give roughly solar-scaled values of $\langle$[Sc/Fe]$\rangle$ = +0.09 (σ = 0.15) and $\langle$[Ni/Fe]$\rangle$ = −0.04 (σ = 0.09). Our results are in agreement with previous studies as we find multiple peaks in the metallicity distribution function at [Fe/H] = −1.75, −1.45, −1.05, and −0.75 and few stars with [Fe/H] < -1.8. These populations represent about 55%, 30%, 10%, and 5% of our sample, respectively. Additionally, we find evidence supporting the idea that the most metal-rich stars are more centrally concentrated, and there appears to be a decrease in the star-to-star metallicity dispersion as a function of increasing distance from the cluster core.

The neutron-capture elements La and Eu yield abundances indicative of strong *s*-process enrichment in all but the most metal-poor stars. We find that nearly all ω Cen stars with [Fe/H] > -1.5 have [La/Eu] $\gtrsim +0.5$, which contradicts the generally *r*-process dominated nature of normal globular cluster stars that have $\langle$[La/Eu]$\rangle \approx -0.25$. Despite the sharp rise in [La/Fe], the Eu abundance remains fairly constant across all metallicities with [Eu/Fe] = +0.19 (σ = 0.23). However, 25% of our sample contains stars with [La/Fe] $\geqslant +1.0$ that are possibly the result of mass transfer in a binary system. These stars are also known to have large Ba4554 indices and are predominantly found at [Fe/H] > -1.3.

Comparing these results with the abundance trends observed in the Galactic halo, disk, bulge, globular clusters, and nearby dwarf spheroidal galaxies indicates the current generation of ω Cen stars share many chemical characteristics found in each of those populations but contain key differences. The elevated [α/Fe] and solar-scaled Fe-peak abundances suggest that Type II SNe have dominated the production of metals in the cluster with almost no contribution from Type Ia SNe. However, we find that at least 40%–50% of stars in our sample have [Na/Fe] and [Al/Fe] ratios that exceed the yields expected from moderately metal-poor SNe. Previous studies have shown that the Na- and Al-enhanced stars are also O-poor, which implies that these stars were polluted by material that has been exposed to high-temperature proton-capture burning. This is corroborated by examining the behavior of [Na/Al] as a function of metallicity. Type II SNe are expected to produce a nearly metallicity independent yield of [Na/Al] ~ -0.2 over $-2 <$ [Fe/H] < -0.5, which matches observations of disk and halo stars, but ω Cen, normal globular cluster, and dwarf spheroidal stars span a range of $-1 \lesssim$ [Na/Al] $\lesssim +0.4$. Therefore, our data strongly support the idea of an additional source of light elements in these environments.

HBB occurring in intermediate-mass AGB stars is a favored location for producing Na and Al while destroying O. Current AGB nucleosynthesis models predict our observed trends, that more Al is produced at low metallicity and more Na produced at high metallicity, and may explain stars with $+0.5 <$ [Al/Fe] $< +1.0$. However, they may not be adequate to reproduce the ∼20% of metal-poor stars with [Al/Fe] > +1, which may require some other source (e.g., in situ mixing or massive rotating stars). What is perhaps most intriguing is that we find evidence for two different subpopulations separated as being either more metal-poor or metal-rich than [Fe/H] ≈ -1.2. Most of the stars with [Fe/H] > -1.2 appear to have formed almost entirely out of AGB ejecta and have [Na/Fe] and [Al/Fe] abundances well above those found in the disk and halo at similar metallicity, while those at [Fe/H] < -1.2 show more of a continuum between strong SN pollution and AGB pollution. Since we did not choose targets based on known chemical properties (e.g., CN strength), it seems that the prevalence of Na- and Al-enhanced stars at higher metallicity is likely not a selection effect. Interestingly, although all ω Cen giants exhibit the same Na–Al correlation found in other globular clusters, the ω Cen stars with [Fe/H]> -1.2 have more Na for a given Al abundance by >0.2 dex compared to what is expected based on the trend seen in normal globular clusters. There is also a mild correlation between La and both Na and Al, but it is unclear how La relates to these elements. The decreasing maximum value of [Al/Fe] at [Fe/H]> -1.2 is not shared by Na and La and suggests a decrease in the [Al/Fe] abundance being added to the cluster's ISM rather than an increase in Fe due to Type Ia SNe.

The sharp increase in the abundance of [La/Fe] and [La/Eu] with increasing metallicity coupled with the relatively long lifetimes of stars thought to produce most of the *s*-process elements is consistent with the generally adopted chemical evolution timescale of ∼2–4 Gyr. However, other stellar systems that evolved over >1 Gyr exhibit the characteristic downturn in

[α/Fe], but this trend is mostly absent in ω Cen stars. Even though it is highly probable that ω Cen did not evolve as a closed box, the apparent preferential retention of Type II versus Type Ia SN ejecta or even the suppression of Type Ia SNe at [Fe/H] > -1 at timescales exceeding 1–2 Gyr remains an important problem.

This publication makes use of data products from the Two Micron All Sky Survey, which is a joint project of the University of Massachusetts and the Infrared Processing and Analysis Center/California Institute of Technology, funded by the National Aeronautics and Space Administration and the National Science Foundation. This research has made use of NASA's Astrophysics Data System Bibliographic Services. R.M.R. acknowledges support from grant AST-0709479 from the National Science Foundation. Support of the College of Arts and Sciences and the Daniel Kirkwood fund at Indiana University Bloomington for C.I.J. is gratefully acknowledged. We thank the referee for his/her thoughtful comments that led to the improvement of the manuscript.

Facilities: CTIO

REFERENCES

Alonso, A., Arribas, S., & Martínez-Roger, C. 1999, A&AS, 140, 261
Alonso, A., Arribas, S., & Martínez-Roger, C. 2001, A&A, 376, 1039
Anders, E., & Grevesse, N. 1989, Geochim. Cosmochim. Acta, 53, 197
Arnett, W. D. 1971, ApJ, 166, 153
Ballero, S. K., Matteucci, F., Origlia, L., & Rich, R. M. 2007, A&A, 467, 123
Bedin, L. R., Piotto, G., Anderson, J., Cassisi, S., King, I. R., Momany, Y., & Carraro, G. 2004, ApJ, 605, L125
Bekki, K., & Norris, J. E. 2006, ApJ, 637, L109
Bellini, A., et al. 2009, A&A, 493, 959
Bensby, T., Feltzing, S., & Lundström, I. 2003, A&A, 410, 527
Bensby, T., Feltzing, S., Lundström, I., & Ilyin, I. 2005, A&A, 433, 185
Blackwell, D. E., & Shallis, M. J. 1977, MNRAS, 180, 177
Boesgaard, A. M., King, J. R., Cody, A. M., Stephens, A., & Deliyannis, C. P. 2005, ApJ, 629, 832
Briley, M. M., Cohen, J. G., & Stetson, P. B. 2004a, AJ, 127, 1579
Briley, M. M., Harbeck, D., Smith, G. H., & Grebel, E. K. 2004b, AJ, 127, 1588
Busso, M., Gallino, R., Lambert, D. L., Travaglio, C., & Smith, V. V. 2001, ApJ, 557, 802
Busso, M., Gallino, R., & Wasserburg, G. J. 1999, ARA&A, 37, 239
Calamida, A., et al. 2005, ApJ, 634, L69
Cannon, R. D., Croke, B. F. W., Bell, R. A., Hesser, J. E., & Stathakis, R. A. 1998, MNRAS, 298, 601
Carretta, E., Bragaglia, A., Gratton, R. G., & Lucatello, S. 2008, arXiv:0811.3591
Carretta, E., Gratton, R. G., Bragaglia, A., Bonifacio, P., & Pasquini, L. 2004, A&A, 416, 925
Castelli, F., Gratton, R. G., & Kurucz, R. L. 1997, A&A, 318, 841
Cavallo, R. M., Suntzeff, N. B., & Pilachowski, C. A. 2004, AJ, 127, 3411
Chieffi, A., & Limongi, M. 2004, ApJ, 608, 405
Choi, E., & Yi, S. K. 2008, MNRAS, 386, 1332
Clarkson, W., et al. 2008, ApJ, 684, 1110
Cohen, J. G., Briley, M. M., & Stetson, P. B. 2002, AJ, 123, 2525
Cowan, J. J., Thielemann, F.-K., & Truran, J. W. 1991, Phys. Rep., 208, 267
Cunha, K., Smith, V. V., Suntzeff, N. B., Norris, J. E., Da Costa, G. S., & Plez, B. 2002, AJ, 124, 379
D'Antona, F., & Ventura, P. 2007, MNRAS, 379, 1431
Decressin, T., Meynet, G., Charbonnel, C., Prantzos, N., & Ekström, S. 2007, A&A, 464, 1029
Denissenkov, P. A., & Herwig, F. 2003, ApJ, 590, L99
Denissenkov, P. A., & Weiss, A. 2004, ApJ, 603, 119
Dickens, R. J., Croke, B. F. W., Cannon, R. D., & Bell, R. A. 1991, Nature, 351, 212
Dinescu, D. I., Girard, T. M., & van Altena, W. F. 1999, AJ, 117, 1792
Elmegreen, B. G. 1999, ApJ, 517, 103
Elmegreen, B. G., Bournaud, F., & Elmegreen, D. M. 2008, ApJ, 688, 67
Fenner, Y., Campbell, S., Karakas, A. I., Lattanzio, J. C., & Gibson, B. K. 2004, MNRAS, 353, 789
Ferraro, F. R., Sollima, A., Pancino, E., Bellazzini, M., Straniero, O., Origlia, L., & Cool, A. M. 2004, ApJ, 603, L81
Francois, P., Spite, M., & Spite, F. 1988, A&A, 191, 267
Fulbright, J. P. 2000, AJ, 120, 1841
Fulbright, J. P., McWilliam, A., & Rich, R. M. 2006, ApJ, 636, 821
Fulbright, J. P., McWilliam, A., & Rich, R. M. 2007, ApJ, 661, 1152
Gehren, T., Liang, Y. C., Shi, J. R., Zhang, H. W., & Zhao, G. 2004, A&A, 413, 1045
Geisler, D., Wallerstein, G., Smith, V. V., & Casetti-Dinescu, D. I. 2007, PASP, 119, 939
Gendre, B., Barret, D., & Webb, N. A. 2003, A&A, 400, 521
Girardi, L., Castelli, F., Bertelli, G., & Nasi, E. 2007, A&A, 468, 657
Gnedin, O. Y., Zhao, H., Pringle, J. E., Fall, S. M., Livio, M., & Meylan, G. 2002, ApJ, 568, L23
Gratton, R. G., Carretta, E., Eriksson, K., & Gustafsson, B. 1999, A&A, 350, 955
Gratton, R., Sneden, C., & Carretta, E. 2004, ARA&A, 42, 385
Gratton, R. G., et al. 2001, A&A, 369, 87
Harris, W. E. 1996, AJ, 112, 1487
Hilker, M., & Richtler, T. 2000, A&A, 362, 895
Hill, V., et al. 2002, A&A, 387, 560
Ivans, I. I., Kraft, R. P., Sneden, C., Smith, G. H., Rich, R. M., & Shetrone, M. 2001, AJ, 122, 1438
Ivans, I. I., Sneden, C., Kraft, R. P., Suntzeff, N. B., Smith, V. V., Langer, G. E., & Fulbright, J. P. 1999, AJ, 118, 1273
James, G., François, P., Bonifacio, P., Carretta, E., Gratton, R. G., & Spite, F. 2004, A&A, 427, 825
Johnson, C. I., Kraft, R. P., Pilachowski, C. A., Sneden, C., Ivans, I. I., & Benman, G. 2005, PASP, 117, 1308
Johnson, C. I., Pilachowski, C. A., Simmerer, J., & Schwenk, D. 2008, ApJ, 681, 1505
Karakas, A., & Lattanzio, J. C. 2007, PASA, 24, 103
Kobayashi, C., Tsujimoto, T., Nomoto, K., Hachisu, I., & Kato, M. 1998, ApJ, 503, L155
Kraft, R. P. 1994, PASP, 106, 553
Kučinskas, A., Hauschildt, P. H., Brott, I., Vansevičius, V., Lindegren, L., Tanabé, T., & Allard, F. 2006, A&A, 452, 1021
Kuijken, K., & Rich, R. M. 2002, AJ, 124, 2054
Lecureur, A., Hill, V., Zoccali, M., Barbuy, B., Gómez, A., Minniti, D., Ortolani, S., & Renzini, A. 2007, A&A, 465, 799
Lee, J.-W., Carney, B. W., & Habgood, M. J. 2005, AJ, 129, 251
Lee, Y.-W., Joo, J.-M., Sohn, Y.-J., Rey, S.-C., Lee, H.-C., & Walker, A. R. 1999, Nature, 402, 55
Magain, P. 1984, A&A, 134, 189
Marino, A. F., Villanova, S., Piotto, G., Milone, A. P., Momany, Y., Bedin, L. R., & Medling, A. M. 2008, A&A, 490, 625
Mateo, M. 2008, The Messenger, 134, 3
Mathews, G. J., & Cowan, J. J. 1990, Nature, 345, 491
McCall, M. L. 2004, AJ, 128, 2144
McWilliam, A. 1997, ARA&A, 35, 503
McWilliam, A., & Rich, R. M. 1994, ApJS, 91, 749
Meylan, G., Mayor, M., Duquennoy, A., & Dubath, P. 1995, A&A, 303, 761
Newsham, G., & Terndrup, D. M. 2007, ApJ, 664, 332
Nomoto, K., Iwamoto, K., Nakasato, N., Thielemann, F.-K., Brachwitz, F., Tsujimoto, T., Kubo, Y., & Kishimoto, N. 1997, Nuc. Phys. A, 621, 467
Nomoto, K., Tominaga, N., Umeda, H., Kobayashi, C., & Maeda, K. 2006, Nucl. Phys. A, 777, 424
Norris, J. E. 2004, ApJ, 612, L25
Norris, J. E., & Da Costa, G. S. 1995, ApJ, 447, 680
Norris, J. E., Freeman, K. C., Mayor, M., & Seitzer, P. 1997, ApJ, 487, L187
Norris, J. E., Freeman, K. C., & Mighell, K. J. 1996, ApJ, 462, 241
Ortolani, S., Renzini, A., Gilmozzi, R., Marconi, G., Barbuy, B., Bica, E., & Rich, R. M. 1995, Nature, 377, 701
Pancino, E., Ferraro, F. R., Bellazzini, M., Piotto, G., & Zoccali, M. 2000, ApJ, 534, L83
Pancino, E., Galfo, A., Ferraro, F. R., & Bellazzini, M. 2007, ApJ, 661, L155
Pancino, E., Pasquini, L., Hill, V., Ferraro, F. R., & Bellazzini, M. 2002, ApJ, 568, L101
Pancino, E., Seleznev, A., Ferraro, F. R., Bellazzini, M., & Piotto, G. 2003, MNRAS, 345, 683
Pilachowski, C. A. 1988, ApJ, 326, L57
Piotto, G. 2008, Mem. Soc. Astron. Ital., 79, 334
Piotto, G., et al. 2005, ApJ, 621, 777
Prantzos, N., & Charbonnel, C. 2006, A&A, 458, 135
Press, W. H., Teukolsky, S. A., Vetterling, W. T., & Flannery, B. R. 1992, Numerical Recipes in FORTRAN: The Art of Scientific Computing (2nd ed.; Cambridge: Cambridge Univ. Press)

Prochaska, J. X., & McWilliam, A. 2000, ApJ, 537, L57
Ramírez, S. V., & Cohen, J. G. 2002, AJ, 123, 3277
Ramírez, I., & Meléndez, J. 2005, ApJ, 626, 465
Reddy, B. E., Lambert, D. L., & Allende Prieto, C. 2006, MNRAS, 367, 1329
Reddy, B. E., Tomkin, J., Lambert, D. L., & Allende Prieto, C. 2003, MNRAS, 340, 304
Reijns, R. A., Seitzer, P., Arnold, R., Freeman, K. C., Ingerson, T., van den Bosch, R. C. E., van de Ven, G., & de Zeeuw, P. T. 2006, A&A, 445, 503
Renzini, A. 2008, MNRAS, 391, 354
Rey, S.-C., Lee, Y.-W., Ree, C. H., Joo, J.-M., Sohn, Y.-J., & Walker, A. R. 2004, AJ, 127, 958
Richer, H. B., Fahlman, G. G., Buonanno, R., Fusi Pecci, F., Searle, L., & Thompson, I. B. 1991, ApJ, 381, 147
Samland, M. 1998, ApJ, 496, 155
Sbordone, L., Bonifacio, P., Buonanno, R., Marconi, G., Monaco, L., & Zaggia, S. 2007, A&A, 465, 815
Schaller, G., Schaerer, D., Meynet, G., & Maeder, A. 1992, A&AS, 96, 269
Shetrone, M. D., Côté, P., & Sargent, W. L. W. 2001, ApJ, 548, 592
Shetrone, M. D., & Keane, M. J. 2000, AJ, 119, 840
Shetrone, M., Venn, K. A., Tolstoy, E., Primas, F., Hill, V., & Kaufer, A. 2003, AJ, 125, 684
Simmerer, J., Sneden, C., Cowan, J. J., Collier, J., Woolf, V. M., & Lawler, J. E. 2004, ApJ, 617, 1091
Smith, G. H. 2008, PASP, 120, 952
Smith, G. H., Shetrone, M. D., Bell, R. A., Churchill, C. W., & Briley, M. M. 1996, AJ, 112, 1511
Smith, V. V., Cunha, K., & Lambert, D. L. 1995, AJ, 110, 2827
Smith, V. V., Suntzeff, N. B., Cunha, K., Gallino, R., Busso, M., Lambert, D. L., & Straniero, O. 2000, AJ, 119, 1239
Smith, V. V., Terndrup, D. M., & Suntzeff, N. B. 2002, ApJ, 579, 832
Sneden, C. 1973, ApJ, 184, 839
Sneden, C., Cowan, J. J., & Gallino, R. 2008, ARA&A, 46, 241
Sneden, C., Kraft, R. P., Guhathakurta, P., Peterson, R. C., & Fulbright, J. P. 2004, AJ, 127, 2162
Sneden, C., Kraft, R. P., Shetrone, M. D., Smith, G. H., Langer, G. E., & Prosser, C. F. 1997, AJ, 114, 1964
Sneden, C., McWilliam, A., Preston, G. W., Cowan, J. J., Burris, D. L., & Armosky, B. J. 1996, ApJ, 467, 819
Sollima, A., Ferraro, F. R., Pancino, E., & Bellazzini, M. 2005a, MNRAS, 357, 265
Sollima, A., Pancino, E., Ferraro, F. R., Bellazzini, M., Straniero, O., & Pasquini, L. 2005b, ApJ, 634, 332
Stanford, L. M., Da Costa, G. S., Norris, J. E., & Cannon, R. D. 2004, Mem. Soc. Astron. Ital., 75, 290
Stanford, L. M., Da Costa, G. S., Norris, J. E., & Cannon, R. D. 2006, ApJ, 647, 1075
Suntzeff, N. B., & Kraft, R. P. 1996, AJ, 111, 1913
Sweigart, A. V., & Mengel, J. G. 1979, ApJ, 229, 624
Timmes, F. X., Woosley, S. E., & Weaver, T. A. 1995, ApJS, 98, 617
van de Ven, G., van den Bosch, R. C. E., Verolme, E. K., & de Zeeuw, P. T. 2006, A&A, 445, 513
van Leeuwen, F., Le Poole, R. S., Reijns, R. A., Freeman, K. C., & de Zeeuw, P. T. 2000, A&A, 360, 472
van Loon, J. T., van Leeuwen, F., Smalley, B., Smith, A. W., Lyons, N. A., McDonald, I., & Boyer, M. L. 2007, MNRAS, 382, 1353
Ventura, P., & D'Antona, F. 2008, MNRAS, 385, 2034
Villanova, S., et al. 2007, ApJ, 663, 296
Wheeler, J. C., Cowan, J. J., & Hillebrandt, W. 1998, ApJ, 493, L101
Woolley, R. R. 1966, R. Obs. Ann., 2, 1
Woosley, S. E., & Weaver, T. A. 1995, ApJS, 101, 181
Yoshii, Y., Tsujimoto, T., & Nomoto, K. 1996, ApJ, 462, 266
Zhang, H. W., Gehren, T., & Zhao, G. 2008, A&A, 481, 489
Zoccali, M., Hill, V., Lecureur, A., Barbuy, B., Renzini, A., Minniti, D., Gómez, A., & Ortolani, S. 2008, A&A, 486, 177
Zoccali, M., et al. 2003, A&A, 399, 931